



HAL
open science

Induction of a strong and long-lasting neutralizing immune response by dPreS1-TLR2 agonist nanovaccine against hepatitis B virus

Myriam Lamrayah, Fanny Charriaud, Manon Desmares, Céline Coiffier, Simon Megy, Evelyne Colomb, Raphaël Terreux, Julie Lucifora, David Durantel, Bernard Verrier

► To cite this version:

Myriam Lamrayah, Fanny Charriaud, Manon Desmares, Céline Coiffier, Simon Megy, et al.. Induction of a strong and long-lasting neutralizing immune response by dPreS1-TLR2 agonist nanovaccine against hepatitis B virus. *Antiviral Research*, 2023, 209, pp.105483. 10.1016/j.antiviral.2022.105483 . hal-03923266

HAL Id: hal-03923266

<https://hal.science/hal-03923266v1>

Submitted on 4 Jan 2023

HAL is a multi-disciplinary open access archive for the deposit and dissemination of scientific research documents, whether they are published or not. The documents may come from teaching and research institutions in France or abroad, or from public or private research centers.

L'archive ouverte pluridisciplinaire **HAL**, est destinée au dépôt et à la diffusion de documents scientifiques de niveau recherche, publiés ou non, émanant des établissements d'enseignement et de recherche français ou étrangers, des laboratoires publics ou privés.

1 Induction of a strong and long-lasting neutralizing immune 2 response by dPreS1-TLR2 agonist nanovaccine against 3 Hepatitis B Virus

4 5 Authors

6 Myriam Lamrayah^a, Fanny Charriaud^a, Manon Desmares^b, Céline Coiffier^a, Simon Megy^c, Evelyne
7 Colomb^a, Raphaël Terreux^c, Julie Lucifora^b, David Durantel^b, Bernard Verrier^a

8
9
10 ^a Colloidal vectors and therapeutic targeted engineering, UMR5305, LBTI, Institut de Biologie et
11 Chimie des Protéines, Université Lyon 1, 7 Passage du Vercors, 69367 Lyon Cedex 07, France.

12 ^b HepVir team, Centre International de Recherche en Infectiologie (CIRI), INSERM U1111, CNRS
13 UMR_5308, University of Lyon (UCBL1), Lyon, France

14
15 ^c ECMO team, UMR5305, LBTI, Institut de Biologie et Chimie des Protéines, Université Lyon 1, 7
16 Passage du Vercors, 69367 Lyon Cedex 07, France.

17
18 * Corresponding author : School of Life Sciences, Ecole Polytechnique Fédérale de Lausanne, SV
19 Station 19, 1015 Lausanne, Switzerland. E-mail address : myriam.lamrayah@epfl.ch.

20 21 Abstract

22
23 Hepatitis B virus remains a major medical burden with more than 250 million chronically infected
24 patients worldwide and 900,000 deaths each year, due to the disease progression towards severe
25 complications (cirrhosis, hepatocellular carcinoma). Despite the availability of a prophylactic
26 vaccine, this infection is still pandemic in Western Pacific and African regions, where around 6% of
27 the adult population is infected. Among novel anti-HBV strategies, innovative drug delivery
28 systems, such as nanoparticle platforms to deliver vaccine antigens or therapeutic molecules have
29 been investigated. Here, we developed polylactic acid-based biodegradable nanoparticles as an
30 innovative and efficient vaccine. They are twice functionalized by (i) the entrapment of Pam₃CSK₄,
31 an immunomodulator and ligand to Toll-Like-Receptor 1/2, and by (ii) the adsorption/coating of
32 myristoylated (2-48) derived PreS1 from the HBV surface antigen, identified as the major viral
33 attachment site on hepatocytes. We demonstrate that such formulations mimic HBV virion with an
34 efficient peptide recognition by the immune system, and elicit potent and durable antibody
35 responses in naive mice during at least one year. We also show that the most efficient *in vitro* viral
36 neutralization was observed with NP-Pam₃CSK₄-dPreS1 sera. The immunogenicity of the derived
37 HBV antigen is modulated by the likely synergistic action of both the dPreS1 coated nanovector
38 and the adjuvant moiety. This formulation represents a promising vaccine alternative to fight HBV
39 infection.
40

41 **Keywords**

42

43 Hepatitis B virus, neutralizing antibodies, PreS1 peptide, TLR agonist, nanoparticle, poly(lactic
44 acid)

45

46 **Highlights**

47

- 48 ● PreS1 peptide derived from HBV surface protein was successfully adsorbed on PLA NP
- 49 ● Vectorized Pam₃CSK₄ does not influence the colloidal characteristics of NP-dPreS1
- 50 ● NP-dPreS1 activates murine lymph nodes after subcutaneous administration
- 51 ● Pam₃CSK₄ adjuvant positively modulates the quality of immune response triggered by NP
- 52 ● NP-Pam₃CSK₄-dPreS1 induces the most efficient murine IgG for *in vitro* neutralization

53 1. Introduction

54

55 Nearly 3.5% of the world population suffer from chronic hepatitis B virus (HBV) (Polaris Observatory
56 Collaborators, 2018) and predictions for the future are not optimistic, as the mortality rate is
57 increasing and outweighing those of tuberculosis, malaria, and HIV (Bray et al., 2018; Graber-
58 Stiehl, 2018). Even though existing prophylactic vaccines widely protect the rich countries
59 benefiting from it, they present some drawbacks that make it difficult to implement in developing
60 countries: cold storage, a strict three-shot immunization schedule, the failing to induce an effective
61 antibody (Ab) response in 5-10% of healthy “non responders” (Saco et al., 2018) and the
62 emergence of vaccine escape strains (Qin and Liao, 2018). New potent vaccines have to be
63 considered via (i) the use of drug delivery systems to optimize the administration (Zhu et al., 2019),
64 (ii) the modification of the antigen (Ag) sequence for a more immunogenic portion, (iii) the
65 adjuvantation to enhance the immune response (Fanning et al., 2019; Lang et al., 2019; Meng et
66 al., 2019). This has been confirmed recently in the course of SARS-CoV-2 countermeasures, when
67 the numerous failed clinical trials have highlighted the importance to generate innovative and
68 highly-immunogenic formulations through efficient systems (Monrad et al., 2021; Peplow, 2021).

69

70 Multiple drug delivery systems (*i.e.* virus-like particles, nanoparticles) and innovative gene-based
71 formulations (DNA/RNA vaccines) have been largely exploited in vaccinology for their added value
72 compared to a conventional soluble Ag (Fries et al., 2020) and thus, for their ability to face a global
73 health emergency, such as the ongoing SARS-CoV-2 pandemic (Brisse et al., 2020). Nanoparticle
74 (NP) systems aim at overcoming the limitations of conventional delivery by : improving the stability
75 and solubility of molecules, facilitating the transport across membranes to modulate the traffic and
76 the delivery of vaccine components throughout the lymphatic tissue (Mitchell et al., 2020; Schudel
77 et al., 2019), thus improving the Ag presentation and overall the prophylactic activity (Fries et al.,
78 2020). By efficiently targeting the lymph nodes (LN), nanovaccines induce a more persistent B cell
79 immune response compared to conventional forms (Singh, 2021). Biodegradable polymeric NP are
80 one of the most extensively studied in the field for their low immunogenicity and biocompatibility
81 and our previous results showed the polylactic acid (PLA) as a great polymer candidate for such
82 scaffolds (Coolen et al., 2019; Pavot et al., 2016; Ressaygue et al., 2017). They offer a versatile
83 platform for vectorization (Pavot et al., 2013) and/or adsorption (Dalzon et al., 2016) of various
84 molecules (Ag, immunomodulators) and are promising candidates for vaccine development
85 (Gutjahr et al., 2016; Peres et al., 2017).

86

87 Yan *et al* elegantly identified the myristoylated oligopeptide (amino acids sequence 2-48) named
88 PreS1 from the large surface protein, as the molecule enabling HBV to enter into the hepatocyte
89 (Yan et al., 2012) through a high-affinity binding with the sodium taurocholate cotransporting
90 polypeptide (NTCP) receptor (Meier et al., 2013). The inhibition of this PreS1-NTCP interaction
91 effectively blocks HBV and hepatitis D virus (HDV) infections (Ni et al., 2014; Ye et al., 2016).
92 Bulevirtide (also known as myrcludex B), the GMP-version of the myristoylated (2-48) PreS1, was
93 recently approved in Europe for HDV treatment (Cheng et al., 2021). Yato *et al* suggested the
94 potential ability of a vaccine Ag containing the preS1 region to overcome the weakness of current
95 hepatitis B vaccines (Yato et al., 2020). Indeed, monoclonal Abs against the conventional HBsAg
96 protein cannot neutralize HBV in case of vaccine escape mutations such as the G145R mutation
97 which causes a conformational change in the HBsAg antigenic loop. This lack of neutralization is
98 not observed with Abs against PreS1/2-48. Two other studies recently highlighted also the added
99 value of using this PreS1 domain by bypassing the host immune tolerance observed with HBsAg
100 vaccines (Bian et al., 2017; Dembek et al., 2018). Inducing specific anti-PreS1 Abs may therefore
101 be optimal when the conventional HBV vaccine targeting the main antigenic region (AR). Here, a
102 derived PreS1 (dPreS1) sequence of the virus was successfully nanovectorized in PLA NP and
103 investigated.

104 As an adjuvant, the Toll-Like-Receptor (TLR) 1/2 agonist Pam₃CSK₄ was included in the
105 nanosystem for an enhanced magnitude and durability of the immune response (Pulendran et al.,
106 2021). The literature demonstrates the efficacy of synthetic TLR ligands on rodents and non-human
107 primates by promoting a more durable and stronger Ab response to vaccination with live or heat-
108 killed viruses (Hennessy et al., 2010; Kasturi et al., 2011). More specifically for HBV, HepLisav-B is
109 an FDA-approved vaccine composed of HBsAg mixed with a synthetic oligonucleotide cytosine
110 phosphor-guanine (CpG) that stimulate innate immunity through TLR9 (Lee and Lim, 2021). In case
111 of TLR2, multiple experimental evidences show the promising adjuvanticity of Pam₃-related ligands
112 as strong inducers of virus-specific T and B cells in mice (Dou et al., 2020; Lee and Park, 2018;
113 Rammensee et al., 2019). Desmares *et al* (Desmares et al., 2022) illustrate recently the direct
114 inhibitory anti-HBV phenotypes induced by this TLR2 ligand itself supporting our assumption of an
115 added value in using Pam₃CSK₄. Despite the numerous preclinical and clinical studies applied to
116 TLR ligands, their mechanisms of action suggest failures related to toxicity issues limiting a human
117 use (Anwar et al., 2019).

118
119 For all these reasons, we propose a highly immunogenic doubly-functionalized NP vaccine against
120 HBV, incorporating both the unique dPreS1 domain and a TLR1/2 ligand for adjuvanticity. We have
121 previously discussed the successful chemical entrapment of Pam₃CSK₄ in PLA NP (Lamrayah et
122 al., 2019). Here, in order to validate the immunological relevance and the effective design of our
123 NP-dPreS1 vaccine, we first performed *in silico* structural and physicochemical modulations. Then,
124 the immune responses elicited by a prime-boost administration were evaluated in comparison with
125 different formulations. The NP-Pam₃CSK₄-dPreS1 (hereafter designated NP-P-dPreS1) system
126 aims at stimulating the production of neutralizing Abs directed specifically against the dPreS1
127 epitope all the while favorably modulating the immune response for an optimal immune protection.
128 Finally, the *in vitro* neutralization capacity of the generated antibodies was tested to evaluate their
129 antiviral efficacy. Overall, this work offers a promising platform for a novel anti-HBV vaccine and
130 maybe a potential strategy to achieve a functional cure in a therapeutic context, as it induces a high
131 level and persistent anti-PreS1 response that could help in clearing circulating HBV virions as well
132 as infected hepatocytes *in vivo* by various mechanisms (e.g., neutralization, ADCC, etc.).

133

134 **2. Materials and methods**

135 **2.1. Preparation and characterization of formulations**

136 PLA NP were prepared by nanoprecipitation technique as previously described (Lamalle-Bernard
137 et al., 2006). Briefly, the polymer was dissolved in acetone and this solution was added dropwise
138 to an aqueous solution under 250 rpm stirring. Organic solvents were then removed under reduced
139 pressure at 30°C with a Rotavapor R-300 (Buchi, France).

140 Pam₃CSK₄ (purchased from InvivoGen, San Diego, CA, USA) was incorporated during the NP
141 synthesis, following the procedure already described (Lamrayah et al., 2019). The final
142 concentration of Pam₃CSK₄ was 2.5 µg/injection.

143 The near infrared DiR XenoLight Fluorescent Dye (DiIC18(7), 1,1'-dioctadecyltetramethyl
144 indotricarbocyanine Iodide), purchased from Perkin Elmer (Waltham, MA, USA), was incorporated
145 during the NP synthesis step at a fluorophore:PLA ratio of 0.02% and was manufactured by
146 Adjuvatis (Lyon, France).

147 The 2-48 AA sequence of the HBV PreS1 peptide with a myristoylation in N-terminal
148 (GTNLSVNPPLGFFPDHQLDPAFRANSNNPDWDFNPNKDHWPPEANKVG) was produced by
149 GenScript Biotech (Piscataway, NJ, USA). The purity was higher than 98% and the observed

150 molecular weight was 5499.5 g/mol. For the preparation of dPreS1 PLA NP, the lyophilized dPreS1
151 was rehydrated in PBS 1X (Thermo Fisher Scientific, Waltham, MA, USA) at the desired
152 concentration and added volume to volume in NP, NP(DiR) or NP-Pam₃CSK₄ suspensions,
153 previously diluted at 20 mg/mL of polymer in DPBS 1X. The passive adsorption reaction occurred
154 within 2 h at room temperature with moderate overhead stirring. The coating efficiency was
155 assessed by measuring the unbound peptide. A certain volume of dPreS1 PLA NP was centrifuged
156 15 min at 15,000 xg and the absorbance of the supernatant was measured at 280 nm using a
157 Tecan i-control Infinite M1000 (Tecan, Männedorf, Switzerland). The results were compared to a
158 calibration curve previously established (correlation coefficient of R²=0.998). The encapsulation
159 efficiency was calculated as the following formula: EE (%) = (1 - amount of dPreS1 in supernatant
160 / Total amount of dPreS1) x 100. The final concentration of dPreS1 was 20 µg/injection.

161 The average hydrodynamic diameter and the size distribution (mentioned as polydispersity index
162 or PDI) of formulations were determined by dynamic light scattering at 25°C and a scattering angle
163 of 173° using a Zetasizer Nano ZS (Malvern, UK). The colloidal suspensions were a hundred time
164 diluted in filtrated 1 mM NaCl solution and each value was the mean of four independent
165 measurements. The electrophoretic mobilities (mentioned as zeta potential) were measured by
166 laser Doppler velocimetry using the same equipment, at a scattering angle of 12.5°.

167 For KLH-dPreS1 formulation, 200 µg of dPreS1 was conjugated with 200 µg of mariculture Key
168 Limpet Hemocyanin (mckLH) in EDC conjugation buffer, following the manufacturer's instructions
169 (Imject™ EDC mckLH Spin Kit, Thermo Fisher Scientific, USA). The mix was incubated for 2 h
170 statically at room temperature. The conjugate was purified by successive desalting steps to remove
171 the non-reacted crosslinker.

172 **2.2. Molecular Modeling**

173 MD simulations were performed using the Amber 14 force field implemented in the Molecular
174 Operating Environment (MOE) software (ChemComp). This type of atomistic simulation allows for
175 the modeling of various system sizes but is less efficient with larger systems, especially when the
176 total number of atoms reaches millions, which is the amount typically found in a 150 nm diameter
177 NP. Thus, in order to mimic the behavior of a PLA NP while keeping the total number of atoms in
178 the simulation under a reasonable limit, we chose to use instead a smooth flat layer of PLA with a
179 35 Å thickness, located in a replicative cell measuring 60x60x120 Å. To simulate the NP PLA
180 surface, we used PLA molecules constructed as linear repetitions of 50 units of Lactic Acid
181 monomers (LA). Those molecules were generated using the "Build" module of the Material Studio
182 software (Biovia). Water molecules were added for the solvation of the replicative cell. The
183 simulation box was then thoroughly minimized using the Forcite module of Material Studio. The
184 PLA molecules and the replicative cell were then exported in .pdb format and imported into the
185 MOE software. Then, a molecular model of the dPreS1 peptide was constructed. As no single
186 relevant template could be found in the PDB database, we used the online software I-TASSER
187 (Iterative Threading ASSEmbly Refinement) from the Zhang Lab ("I-TASSER server for protein
188 structure and function prediction," n.d.). Five models were computed using the software default
189 options, and the best one was further imported into MOE. The lipidic myristoyl anchor of dPreS1
190 was constructed using the MOE Build module and the molecule was briefly minimized using the
191 Amber 14 EHT force field. The final model was added to the PLA periodic cell and located close to
192 the PLA surface. The geometry of all the molecules, bonds and charges were checked using the
193 Structure Preparation tool in MOE, to start molecular simulations. Water molecules, Na⁺ and Cl⁻
194 ions were added to simulate a 0.1 M ionic force, and pH was set at 7.4. The total number of atoms
195 in the simulation cell was 38,403. Standard Amber 14 EHT parameters were used for the molecular
196 dynamics. A quick minimization was performed prior to the start of the MD simulations. After a

197 preliminary equilibration phase, a 200 ns molecular simulation was performed. A frame was saved
198 every 20 ps, leading to a total number of 10,000 frames.

199

200 **2.3. Docking**

201

202 The docking experiments were performed between the CSK4K4 peptidic part of the Pam₃CSK₄
203 lipopeptide and the 47 AA sequence of PreS1. The protocol involved a first global approach step
204 of peptide/protein docking using the Haddock (High Ambiguity Driven protein-protein DOCKing)
205 web server (van Zundert et al., 2016) and the Cluspro 2.0 web server ("ClusPro 2.0: protein-protein
206 docking," n.d.). No constraints about the binding area were specified and all the residues of the
207 CSK4K4 peptide were treated as flexible. The two servers produced 42 poses, which were
208 selected and sent for further docking refinement to the Rosetta docking software, version 3.12
209 (Chaudhury and Gray, 2008). All initial Haddock and Cluspro pose were refined 100 times with
210 Rosetta, leading to 4200 refined poses. The top ten results were evaluated with the Rosetta 2015
211 scoring function (Park et al., 2016) and exhibited a mean average reweighted score of 60.1 Rosetta
212 Energy Units.

213

214 **2.4. Electron microscopy observations**

215

216 Morphology of formulations was visualized through a transmission electron microscope (JEM-
217 2100F, JEOL, Japan). For sample preparation, NP solutions were diluted ten times in water and
218 deposited on a grid. The excess liquids were absorbed using filter paper and the grids were
219 negatively stained by sodium silicotungstate for contrast. Images were recorded at a magnification
220 between x10K and x20K.

221

222 **2.5. *In vivo* imaging of fluorescent NP biodistribution**

223 Ten-week-old SKH1 female mice (n=4 per group) were bred at Charles River Laboratories
224 (L'Arbresle, France) and housed at the AniCan animal facility of the CRCL (Cancer Research
225 Center of Lyon, France). The experiments were approved by the relevant local ethics committee
226 (CECCAPP_CLB_2017_006) and were conducted according to the rules for the care and use of
227 laboratory animals. The mice received a single subcutaneous injection in the neck of 0.96 μM
228 DiR/mouse loaded in NP or in dPreS1-NP, corresponding to 20 μg of dPreS1/mouse (injection
229 volume: 100 μl). Whole body fluorescence was recorded at determined time points (2, 24 h and 7
230 days after injection) using the FMT4000 fluorescence tomography imaging system (Perkin Elmer,
231 USA). On the day of imaging, mice were anesthetized under 4% isoflurane and positioned in the
232 FMT system imaging chamber. Filter set was chosen depending on the fluorophore parameters,
233 with an excitation at 750 nm and a collection at 782 nm. The collected fluorescence data were
234 reconstructed by TrueQuant software for the quantification of three-dimensional fluorescence
235 signals. Acquired images were analyzed by drawing regions of interest (ROI). The total amount of
236 fluorescence (in pmoles) per ROI was generated for all studies, and then percentage of residual
237 fluorescence was calculated as: residual fluorescence (%) = [amount of fluorescence at tx / amount
238 of fluorescence at t0] x 100.

239 **2.6. Lymph nodes immunofluorescence staining**

240 Seven-to-eight-week-old mice were divided into five groups of nine animals and received a single
241 immunization of the different formulations in a 100 μl final volume of PBS 1X, subcutaneously above
242 the left inguinal LN. Mice were retro-orbitally bled before immunization and 7-, 14-, 21- and 28-days
243 post-immunization. Three mice of each group were euthanized at 7-, 14-, 21- and 28-days post-
244 immunization to harvest the draining inguinal LNs. They were snap frozen in cryomolds full of

245 Optimal Cutting Temperature compound (Tissue-Tek O.C.T, Sakura Finetek, USA) placed on dry
246 ice and stored at -80°C until cryosection. Serial sections, 8 µm thick, were collected through each
247 LN using a cryostat microtome (cryostat CM3050, Leica Biosystems, Germany). The central section
248 and the two sections spaced 250 µm apart were fixed on glass slides with acetone. They were first
249 incubated with a rat anti-mouse IgD primary Ab (Biolegend, San Diego, CA, USA) to detect B cells
250 follicles and with biotinylated PNA (Vectors Laboratories, Burlingame, CA, USA) to detect GC. They
251 were then incubated with goat anti-rat IgG secondary Ab conjugated with Alexa Fluor 488 (Thermo
252 Scientific, Rockford, IL, USA) to reveal anti-IgD (green), and with Streptavidin conjugated with
253 DyLight 550 (Thermo Scientific, Rockford, IL, USA) to reveal biotinylated PNA (red). Images of LN
254 sections were captured using an inverted microscope (Nikon Ti-E microscope, Nikon Instruments
255 Inc., Melville, NY, USA) equipped with a 4x objective. Measurements of B cells and GCs areas
256 were carried out using Image J software (U. S. National Institutes of Health, Bethesda, MD, USA).
257 GCs were manually counted.

258 **2.7. CXCL13 ELISA**

259 The mouse CXCL13/BLC/BCA-1 DuoSet (R&D Systems, USA) was used for quantification of
260 CXCL13 in sera samples, according to the manufacturer's recommendations. Briefly, ninety-six-
261 well Nunc maxisorp plates were coated with 100 µL of Capture Ab at 1 µg/mL, overnight at room
262 temperature. Capture Ab excess was eliminated and plates were washed 3 times with PBS/0.05%
263 Tween-20 (PBS-T20) using a Thermo Scientific autoplate washer. Plates were blocked with 300
264 µL of Block buffer (R&D Systems, USA) for 1 h at room temperature, to prevent non-specific binding
265 of the CXCL13 protein. Fresh serum samples from immunized mice were diluted five times in
266 Reagent Diluent (RD) (R&D Systems, USA). A seven-point standard range using two-fold serial
267 dilutions in RD of the recombinant mouse BLC/BCA-1 Standard was realized. Then, 100 µL of each
268 sample and standard in duplicate were incubated on washed plates for 2 h at room temperature.
269 Wells were washed and incubated 2 h at room temperature with Detection Ab diluted at 25 ng/mL
270 in RD. Plates were washed again and incubated with 100 µL per well of diluted Streptavidin-HRP
271 in RD (1:200) for 20 min at room temperature, in the dark. Plates were washed again, revealed
272 using 100 µL per well of tetramethylbenzidine (TMB) substrate (BD BioSciences, USA) and stopped
273 using 2N H₂SO₄ (Merck, USA). The optical density (OD) at 450 nm (OD₄₅₀) with a correction at 620
274 nm was measured using a Thermo Scientific plate reader spectrophotometer.

275 **2.8. Immune evaluation of formulations in naive mice**

276 CB6F1 female mice were bred at Charles River Laboratories (L'Arbresle, France) and housed at
277 the Plateau de Biologie Expérimentale de la Souris (PBES, Lyon, France). The experiments were
278 approved by the relevant local ethics committee (CECCAPP_ENS_2017_017) and were conducted
279 according to the rules for the care and use of laboratory animals.

280 Seven-to-eight-week-old mice were equally distributed into six groups in the indicated experimental
281 groups. They were subcutaneously immunized (above the left inguinal LN) with NP-dPreS1, NP-
282 Pam₃CSK₄-dPreS1, soluble dPreS1, NP as negative control and KLH-dPreS1 as positive control.
283 The injection scheme followed a prime boost injection strategy, based on Aditec consortium
284 protocol for harmonization with three immunizations each three weeks. A sixth group received a
285 retro-orbitally intravenous injection of NP-Pam₃CSK₄-dPreS1, following the same scheme of
286 immunization. Components were administered equally for each group, namely 2.5 µg of dPreS1,
287 20 µg of Pam₃CSK₄, 10 mg/mL of PLA and all formulations were diluted in PBS 1X for a 100 µl final
288 volume of injection.

289 Then, a heterologous boost was performed at W27, with a unique formulation subcutaneously
290 injected for all groups, meaning dPreS1 NP. Control groups received a homologous injection,

291 meaning NP and KLH-dPreS1 respectively as negative and positive controls, to maintain the
292 reference consistent.

293 Mice were retro-orbitally bled before immunization and at determined times (W2, 4, 6, 8, 11, 13,
294 17, 22, 27, 32, 44 and 47 weeks post-immunization). The blood samples were heated 30 min at
295 37°C for coagulation, then centrifuged twice 10 min at 16,000 ×g and sera were stored at -20°C
296 for further analyses. Mice were weighted regularly to verify the potential general toxicity of immune
297 stimulation in naive organisms and the evolution rate for each group was measured as: ((W47
298 weight - W7 weight)/ W7 weight) x 100 = evolution rate (%). Mice were sacrificed at W47 by cervical
299 dislocation.

300 **2.9. dPreS1 specific IgG ELISA**

301 Collected sera were tested for the quantification of dPreS1 specific IgG, IgG1 and IgG2a by
302 enzyme-linked immunosorbent assay (ELISA). Ninety-six-well Nunc maxisorp plates
303 (ThermoFisher Scientific, USA) were coated with 100 µL of dPreS1 at 1 µg/mL, overnight at room
304 temperature. The dPreS1 excess was eliminated and plates were blocked with 200 µL of 10% non-
305 fat dry milk in PBS for 1 h at 37°C to prevent non-specific binding of the Abs. Plates were washed
306 3 times with PBS/0.05% Tween-20 (PBS-T20) using a Thermo Scientific autoplate washer. Serum
307 samples from immunized mice were serially diluted in Dulbecco's PBS (DPBS) containing 1% (w/w)
308 of Bovine Serum Albumin (Euromedex, Souffelweyersheim, France). Then, 100 µL of each sample
309 in duplicate were incubated on blocked plates for 1 h at 37°C. Wells were washed three times and
310 incubated 1 h at 37°C with anti-mouse IgG-HRP (horseradish peroxidase) conjugate (1:10,000)
311 from Southern Biotech, Birmingham, AL, USA (ref 1030-05). Plates were washed again, revealed
312 using 100 µL per well of tetramethylbenzidine (TMB) substrate (BD Biosciences, USA) and stopped
313 using 1N sulfuric acid. The optical density (OD) at 450 nm with a correction at 620 nm was
314 measured using a microplate reader spectrophotometer (Multiskan FC, Thermo Fisher, USA). The
315 limit of detection was evaluated using an unconjugated mouse monoclonal anti-Hep B PreS1 (ref
316 SC-57761) from Santa Cruz Biotechnology, Inc. (Dallas, TX, USA).

317 Sera from W0, 11, 22, 32 and 47 were also evaluated for the presence of dPreS1 specific IgG1
318 and IgG2a, using the same protocol than for total IgG, except the last incubation with IgG1-HRP
319 (ref 1070-05) or IgG2a-HRP (ref 1080-05) conjugate, both from Southern Biotech.

320 The avidity indices of IgG at W6, 11, 22, 32 and 47 were determined by the Ab-Ag binding
321 resistance to 8M of urea. Samples were prediluted to give an OD₄₅₀ readout of between 1.0 and
322 1.5, with a correction at 620 nm, and were added to dPreS1 coated plates. Then, they were washed
323 three times with either PBS-T20 or 8 M urea in PBS-T20, before incubating with anti-mouse IgG-
324 HRP. Samples were developed with TMB as described above. The avidity index (in percent) was
325 calculated as the ratio of absorbance of bound Ag in the plate with and without urea as denaturing
326 reagent = (OD urea/OD PBS-T20) x 100. Index values exceeding 50% were ascribed a high avidity,
327 those between 30 and 50% were ascribed intermediate avidity, and those below to 30% were
328 ascribed a low avidity.

329 **2.10. Cell culture**

330 *In vitro* experiments were performed with a HepaRG cell line (Gripon et al., 2002). Cells were
331 maintained in William's E medium (Life technologies, USA) supplemented with 10% fetal calf serum
332 (FCS) (Eurobio, Hyclone), 100 U/mL of penicillin and 100 µg/mL streptomycin (Gibco, Life
333 technologies, USA), 2 mM GlutaMAX (Gibco, Life technologies, USA), 5 µg/mL of human insulin
334 solution (Sigma-Aldrich, USA) and 5.10⁻⁵ M hydrocortisone hemisuccinate (Serb, France) at 37°C

335 in humidified incubator and 5% CO₂ for two weeks. Two additional weeks are needed for
336 differentiation in standard medium supplemented with 1.8% DMSO (Sigma-Aldrich, MO, USA).

337 **2.11. Neutralization of HBV by mice antisera**

338 Sera from W11, 27 and 47 were diluted into infectious mediums. This last medium was prepared
339 using a differentiation medium containing 4% PEG 8000 (Sigma-Aldrich, MO, USA) and infected
340 with HBV genotype D inoculum prepared from HepAD38 (Lucifora et al., 2018). The infectious
341 medium containing immunized mice sera were maintained during 16 h on HepaRG cells at 37°C
342 and 5% CO₂. Cells were then washed with PBS and the medium of differentiation was added. All
343 *in vitro* experiments were stopped one week after infection and treatment with immunized mice
344 sera. Myrcludex was used as positive control (0.5 ng/mL and 5 ng/mL) after determination of IC50
345 and IC90 on studied cell lines.

346 **2.12. HBe antigen ELISA**

347 From cell culture supernatants, secreted HBeAg and the amount produced were analyzed by
348 ELISA, using a chemiluminescence immunoassay kit (Autobio, China) according to the
349 manufacturer's instructions.

350 **2.13. Statistical analyses**

351 Statistical analyses were performed using GraphPad Prism Version 9.0 software. For each dataset,
352 normality or lognormality was assessed via d'Agostino & Pearson test or Shapiro-Wilk when n was
353 too small and further analyzed accordingly. P<0.05 was considered significant. Differences
354 between groups were analyzed as described in figure legends.

355 **3. Results**

357

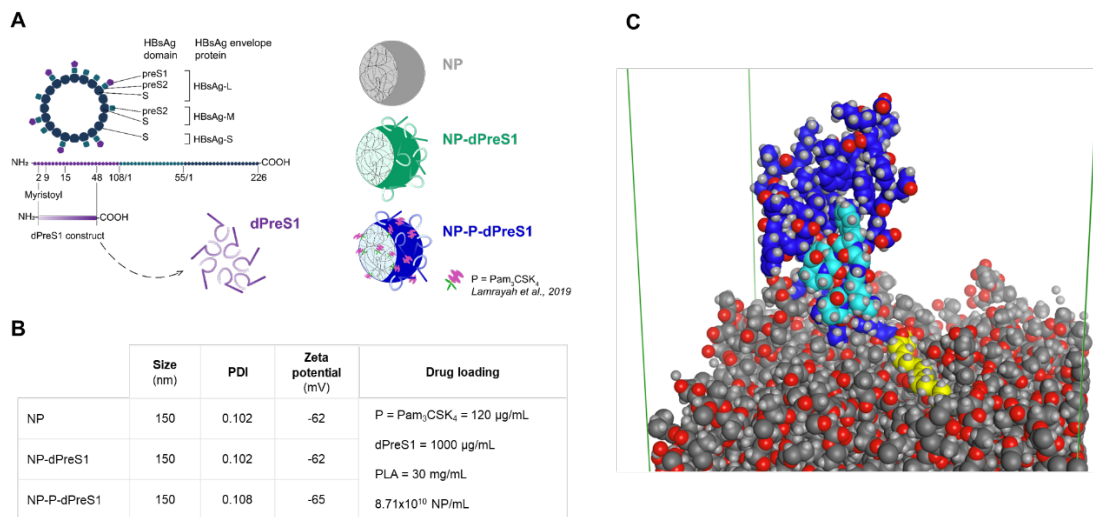
358 **3.1. Design and molecular dynamics studies of HBV-specific NP formulations**

359

360 PLA NP were prepared according to an adjuvant-free nanoprecipitation method (Lamalle-Bernard
361 et al., 2006) and Pam₃CSK₄ was simultaneously entrapped in PLA NP as previously described
362 (Lamayah et al., 2019). Secondly, dPreS1 peptide (2-48 AA construct from a consensus sequence
363 with a N-terminal myristoylation) was added at the surface of the NP by passive adsorption (Dalzon
364 et al., 2016; Pavot et al., 2016). The functionalization of PLA NP by Pam₃CSK₄ and dPreS1 did not
365 significantly change the colloidal size (150 nm), the surface charge (-65 mV) and the dispersity
366 (0.1) (Fig. 1B). Additionally, the NP morphology observed by transmission electron microscopy was
367 also unchanged (Fig. S1). For the drug loading, the encapsulation efficiency of Pam₃CSK₄ was
368 100%, as previously described by the authors (Lamayah et al., 2019), for a 90% adsorption
369 efficiency of dPreS1 (passively measured by the absorbance of the unbound peptide, unshown
370 data). The weights ratio of Pam₃CSK₄, dPreS1 and PLA in the final formulation was fixed at
371 0.12:1:30.

372

373



374
 375 **Fig. 1. NP formulations synthesis was validated and molecular dynamics confirmed the**
 376 **absence of interaction between vectorized dPreS1 and TLR2 agonist. (A)** dPreS1 construct
 377 (2-48 AA with N-ter myristoylation) is derived from the HBsAg-L surface protein. **(B)** Standard
 378 colloidal properties of formulations (size, PDI and surface charge) were verified in order to control
 379 the homogeneity and stability. **(C)** Picture extracted from video S1 at the end of the dPreS1-PLA
 380 surface interaction simulation showing that the biologically relevant epitope of dPreS1 (9-15 AA
 381 sequence, showed in cyan) has a stable conformation and is totally accessible for intermolecular
 382 interactions after the adsorption. The lipidic anchor is in yellow, the rest of the peptide in dark blue,
 383 PLA chains in dark grey, red and light grey for carbon, oxygen, and hydrogen atoms respectively.
 384 The boundaries of the periodic cell are highlighted in dark green. *PDI = polydispersity index.*
 385

386 The PreS1 domain of HBsAg (Fig. 1A) is known to specifically bind to the NTCP receptor located
 387 at the basolateral side of hepatocytes, allowing the viral entry to the cell. More precisely, both the
 388 myristoylated tail (on glycine residue at position 2) and the highly conserved motif 9-NPLGFFP-15
 389 are crucial for receptor binding and infectivity (Glebe et al., 2005). The behavior of the dPreS1
 390 peptide onto the surface of the PLA NP was thus investigated by performing Molecular Dynamics
 391 (MD) simulations. Previously published molecular modeling studies evidenced the major role of
 392 fatty acid chains for the interaction of biological molecules with PLA NP (Lamrayah et al., 2019;
 393 Megy et al., 2020). Consequently, the MD was initiated with the lipidic anchor of dPreS1 (myristic
 394 acid) directly facing the PLA surface. After a preliminary equilibration phase, a 200 ns molecular
 395 simulation was performed. As illustrated in the video (Video S1), the biologically relevant epitope
 396 (9-15 NPLGFFP, in cyan) was not entirely accessible for intermolecular interactions at first, and
 397 progressively undergone several adjustments in its conformation, leading to an improved
 398 accessibility of the relevant epitope after 100 ns of simulation time. The simulation showed the
 399 binding process is possible, and the interaction between dPreS1 and PLA NP evidenced the
 400 stabilization of the epitope in an accessible and opened conformation (Fig. 1C). Noteworthy, the
 401 lipidic anchor stayed in close contact with the PLA chains during the complete simulation without
 402 penetrating the layer, and both their respective conformations were slightly modified, suggesting
 403 hydrophobic interactions. Previous findings demonstrated that the three palmitic chains of
 404 Pam₃CSK₄ are buried into PLA surface, limiting hindrance of both lipidic parts in the final formulation
 405 (Lamrayah et al., 2019). Concerning both peptidic parts, the absence of interactions which could
 406 lead to unexpected results in terms of epitope stability or accessibility had to be verified. In this
 407 regard, docking experiments were performed between the CSK₄ peptidic part of Pam₃CSK₄ and
 408 the 47 AA sequence of dPreS1. All the results exhibited high positive scores, with a top ten average
 409 reweighted score of 60.1 Rosetta Energy Units, demonstrating that there is absolutely no possible

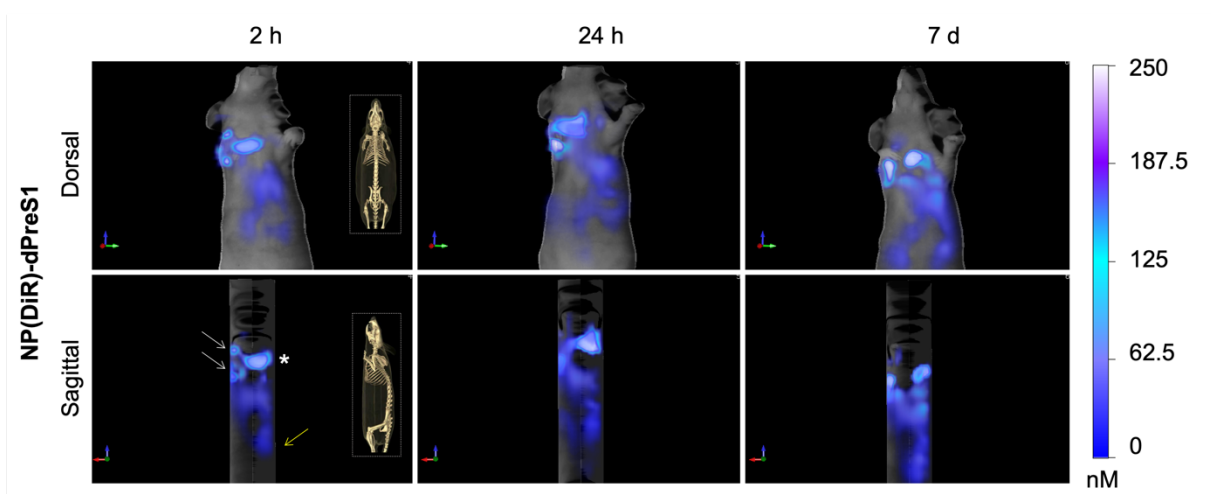
410 interaction between the peptides of the respective molecules (data not shown). As a result, dPreS1
411 and Pam₃CSK₄ did not interact in our system and thus, neither the structure nor the stability of the
412 dPreS1 epitope could be affected by the presence of Pam₃CSK₄. Thus, the chemical stability of the
413 NP-P-dPreS1 formulation was validated and results confirm that the relevant epitope (9-15
414 NPLGFFP) is unchanged and available for recognition by the lymphatic system.

415 416 **3.2. PLA NP efficiently accumulates in the draining lymph nodes and the TLR adjuvant** 417 **influences the kinetics of germinal center formation** 418

419 The importance of germinal center (GC) formation for generating a high-quality and robust Ab
420 response is largely highlighted in the literature (Arulraj et al., 2019; Victora and Nussenzweig,
421 2012). Here, since the antiviral strategy is based on the induction of a strong neutralizing Ab
422 response, it appears essential to explore the early uptake of the formulations following
423 subcutaneous (s.c) administration as well as the subsequent effects in the secondary lymphoid
424 organs (*i.e.* LN). Recent studies have demonstrated the ability of nanovectors to reach the LN after
425 s.c injections (Havenar-Daughton et al., 2019; Singh, 2021). Precisely, NP with a diameter of 100
426 nm and more are entrapped at the injection site by peripheral DCs available in the local interstitial
427 matrix and carried to LN for B cell presentation (Schudel et al., 2019). Thus, the lymphatic
428 biodistribution after s.c administration of the PLA nanovaccines was monitored, and the GC
429 formation, underlying the immune activation within the draining LNs (dLN), was assessed.

430
431 For this, the biodistribution profile of fluorescent PLA NP vectorizing the near infrared DiR probe
432 was investigated using a whole-body 3D fluorescence tomography. These fluorescent NP(DiR) are
433 similar to the active nanovaccine candidates NP(DiR)-dPreS1 in terms of physicochemical
434 characteristics (Fig. S2A) and in the elimination kinetic profile (Fig. S2B and S2C). SKH1 mice were
435 monitored for seven days after a unique s.c injection in the neck region and the detected
436 fluorescence was quantified at 2, 24 hours and 7 days post injection. Noteworthy, the choice of
437 both a hairless strain and a near infrared probe prevented the bias of autofluorescence. A whole-
438 body observation following two axes (dorsal and sagittal) revealed an efficient diffusion and
439 accumulation of the NP to the dLN (Fig. 2). More specifically, these data showed the PLA
440 nanoplatform yields a prolonged and diffused uptake through the lymphatic system, reaching the
441 dLN from 2 hours onwards. The analysis 7 days post immunization also highlighted the persisting
442 biokinetic profile of the NP at the injection site as well as the greater diffusion to non-dLN.

443



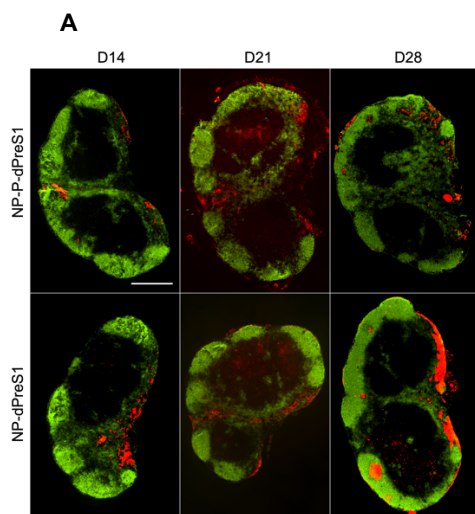
444
445 **Fig. 2. Biodistribution profile of the fluorescent NP-dPreS1 following subcutaneous**
446 **administration shows prolonged retention time and diffusion.** A single s.c injection (neck
447 region, the injection site is shown by the asterisk) was performed on SKH1 female mice with
448 fluorescent NP(DiR)-dPreS1. The fluorescence intensity (750/780 nm) was monitored for 7 days

449 using FMT imaging (Fluorescence Molecular Tomography, FMT4000, Perkin Elmer). Two
450 observation axes were imaged to prove the high penetration score of the fluorescent PLA NP after
451 s.c administration: through the lymphatic system, PLA NP can reach the proximal (white arrows)
452 and distal (yellow arrow) LN.

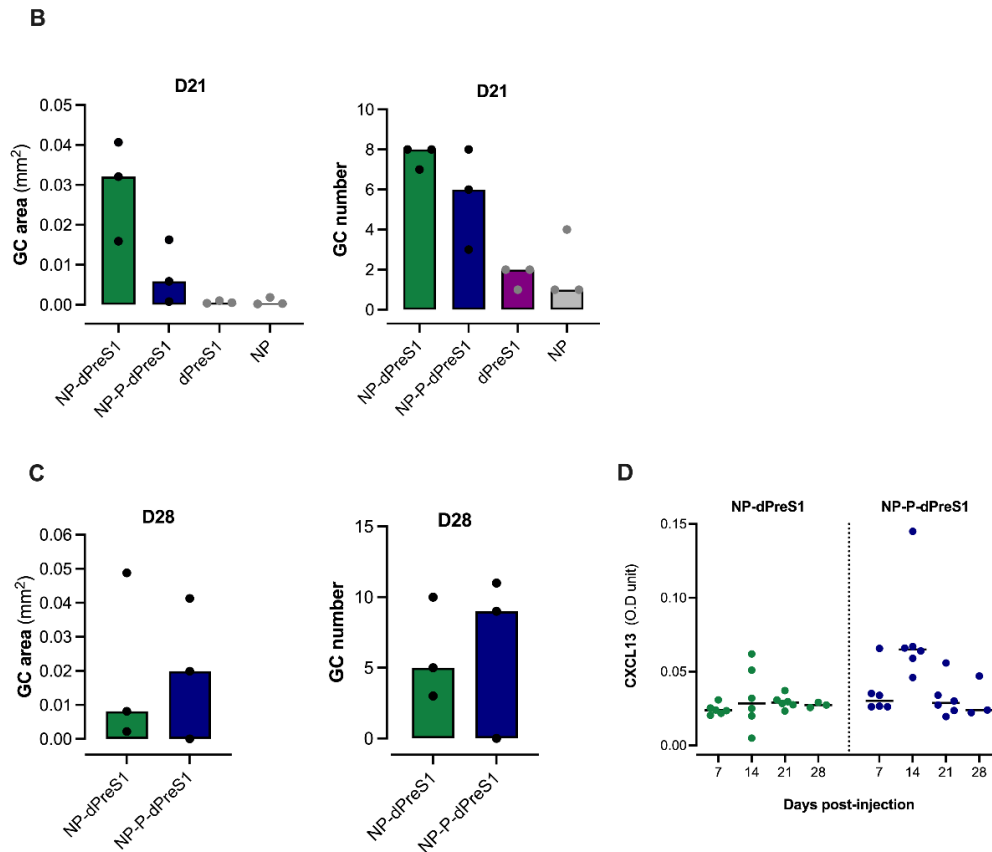
453
454 The first immunization in a protein prime-boost regimen is critical for the subsequent unfolding of
455 the immune response. To confirm the nanovaccine draining uptake and validate the immune
456 activation in LN, CB6F1 mice were immunized once subcutaneously with NP-dPreS1 or NP-P-
457 dPres1 formulations and LN were harvested at predetermined time points for histological analyses
458 (Fig. 3A). NP and soluble dPreS1 injections were both used in control groups. Classically, the GC
459 formation kinetic is described as fully established 7 days after immunization by a soluble Ag (De
460 Silva and Klein, 2015), but considering the prolonged retention effect of nanoparticulate
461 formulations, three mice per group were euthanized at days 14, 21 and 28 post-immunization for a
462 more precise understanding of the biokinetics. The draining inguinal LNs were stained to identify
463 the follicular B cells (using IgD Ab) and the mature GCs (using peanut agglutinin (PNA)). NP-
464 dPreS1 showed a GC response at day 21 post-immunization (Fig. 3B) which decreased at day 28
465 when in parallel it appeared for NP-P-dPreS1 (Fig. 3C).

466
467 To understand this delay, the B-cell-recruiting factor CXC chemokine ligand 13 (CXCL13)
468 expression was monitored in mice serum. This chemokine plays an important role in B cell follicle
469 migration (Havenar-Daughton et al., 2016). Serum levels of CXCL13 increased at day 14 only for
470 NP-P-dPreS1 (Fig. 3D).

471
472



473
474



475
476
477
478
479
480
481
482

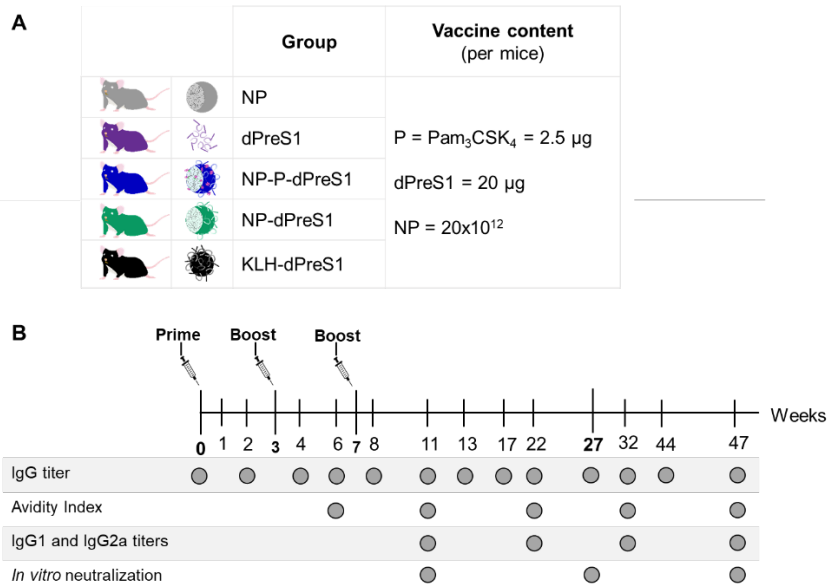
Fig. 3. Draining lymph node responses after a unique s.c administration reveals distinct GC kinetics and numbers. (A) Microscopic observation of GC formation over time. LN were harvested and some cryosections were stained with anti-IgD for follicular B cells (*green*) and PNA for GCs (*red*). Scale bar = 500 μ m. (B) Analyses and number of GC area 21 days after immunization. (C) Analyses and number of GC area 28 days after immunization, only for nanovaccines (NP-dPreS1 and NP-P-dPreS1). (D) Blood levels of CXCL13 monitored during 28 days.

483
484

3.3. Nanovaccines provides a long-lasting and strong humoral response in naïve mice

485
486
487
488
489
490
491
492

Next, to assess the ability of the nanovaccines to induce a specific anti-dPreS1 response, an immunization assay with naïve mice following a prime boost regimen was performed and the serum IgG titers were longitudinally investigated over one year. CB6F1 female mice were randomly distributed ($n=6$ per group) and were subcutaneously immunized three times each three weeks as described in Methods and in Fig. 4A. NP-dPreS1 and NP-P-dPreS1 nanovaccine candidates were compared with soluble dPreS1, KLH-dPreS1 (as positive immunogenic control) and NP (as vector control) (Fig. 4B).



493

494

495

496

497

498

499

500

501

502

503

504

505

506

507

508

509

510

511

512

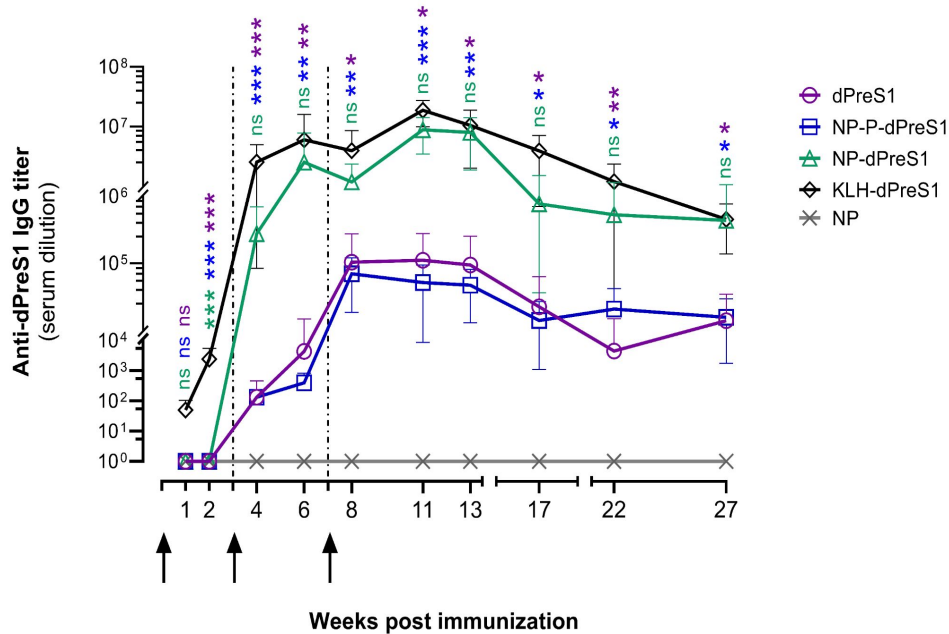
513

514

515

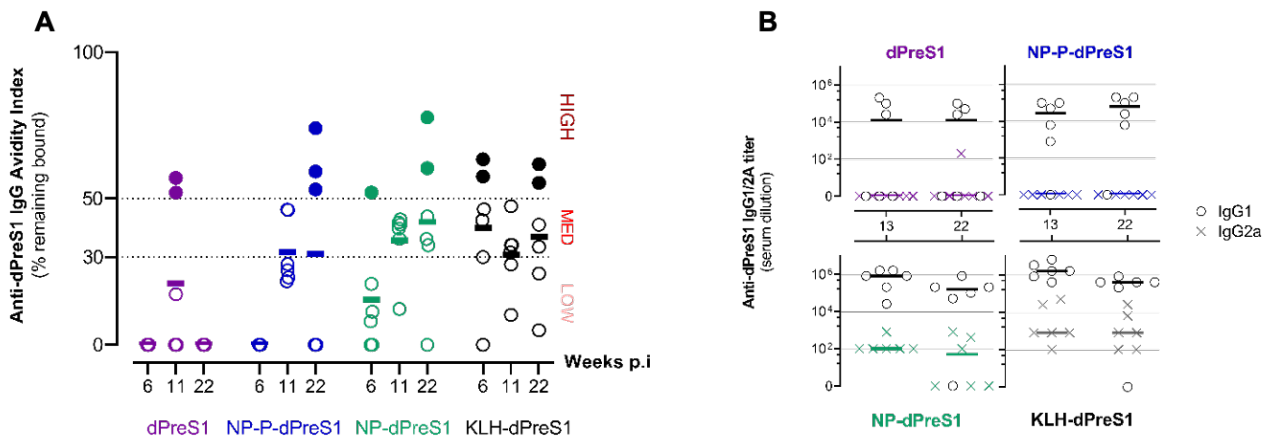
Fig. 4. Detailed study design. (A) Five experimental treatments were formulated and immunologically evaluated on naive CB6F1 mice. At times of injection, all formulations had equivalent quantities of NP ($20 \cdot 10^{12}$ /mouse), Pam₃CSK₄ (2.5 µg/mouse) and dPreS1 (20 µg/mouse). NP and KLH-dPreS1 conditions respectively represent negative and positive controls. **(B)** Mice were kept in experiment during 47 weeks with regular blood analyses to investigate the immune responses after NP-based formulation injections. The following immune parameters were monitored: total anti-dPreS1 IgG, IgG1 and IgG2a titers, Ab avidity, *in vitro* HBV neutralization efficacy of the antisera. At W27, a final heterologous s.c boost was performed: all mice received the NP-dPreS1 formulation (yellow boost) except for the control groups (KLH-dPreS1 and NP) which received their own formulations. Mice were euthanized at W47 using cervical dislocation.

The NP-dPreS1 formulation rapidly elicited elevated titers of anti-dPreS1 IgG reaching about 10^7 during the plateau phase and remaining still high (10^6) after six months with insignificant difference compared to the positive immunogenic control KLH-dPreS1 (Fig. 5). Soluble dPreS1 was immunologically recognized, which is in accordance with the literature (Bian et al., 2017), but still elicited significantly lower quantities of anti-dPreS1 IgG titers reaching 10^5 during the plateau phase to decrease by one log six months later. Noteworthy, only 50% of the subjects (3/6) responded to immunization in this group (Fig. S5). The addition of Pam₃CSK₄ as an adjuvant in NP forms decreased by two log the induced specific IgG quantities, overlapping the IgG profile of the dPreS1 group.



516
 517 **Fig. 5. For each group, anti-dPreS1 IgG titer was analyzed on mice sera from W1 post**
 518 **immunization onwards.** A dPreS1 specific in-house ELISA (limit of detection = 0.01 µg/mL, see
 519 Fig. S3) was developed. Each symbol represents an individual animal and full bars indicate the
 520 mean of the group for each timepoint. Statistical analysis was performed by ANOVA test with
 521 multiple comparisons and Dunnett's correction using positive control KLH-dPreS1 condition as
 522 reference. $\alpha=0.05$, * $p<0.05$, ** $p<0.005$, *** $p<0.001$, ns = not significant.
 523

524 To qualitatively describe the immune responses, the avidity and isotype of induced IgGs were
 525 evaluated. The avidity index represents the total binding strength of the Ag-Ab interaction and can
 526 vary during the immune response depending on the affinity maturation and clonal selection
 527 processes. Indexes were measured by the ability of the mice antisera to remain in binding with
 528 dPreS1 in the presence of 8M urea as detergent (Badamchi-Zadeh et al., 2016). All formulations
 529 had low mean avidity indexes after the first immunization, except for KLH-dPreS1 group which
 530 showed an intermediate mean index, unchanged until W22. Since KLH is described as strongly
 531 immunogenic due to its high molecular mass, the constant intermediate avidity level is not
 532 surprising (Harris and Markl, 1999; Swaminathan et al., 2014). In contrast, the Ab avidity increased
 533 progressively with time and reached an intermediate mean index for both NP-dPreS1 (31%) and
 534 NP-P-dPreS1 (42%) at W22. Interestingly, when considering results individually, NP-dPreS1
 535 formulation induced the most homogenous response at W22 (5/6 mice over 30%) compared to NP-
 536 P-dPreS1 which offered the highest response (3/6 mice over 50%). Soluble dPreS1 induced Ab
 537 with low or none average avidity (Fig. 6A). Further characterization indicates the Th1/Th2 skewing
 538 of the immune response via IgG1/IgG2a titer quantification. IgG1 isotype was predominant for all
 539 groups, suggesting a major Th2 cell polarization for all vaccine regimens (Bretscher, 2019) (Fig.
 540 6B).



541
542
543
544
545
546
547
548
549

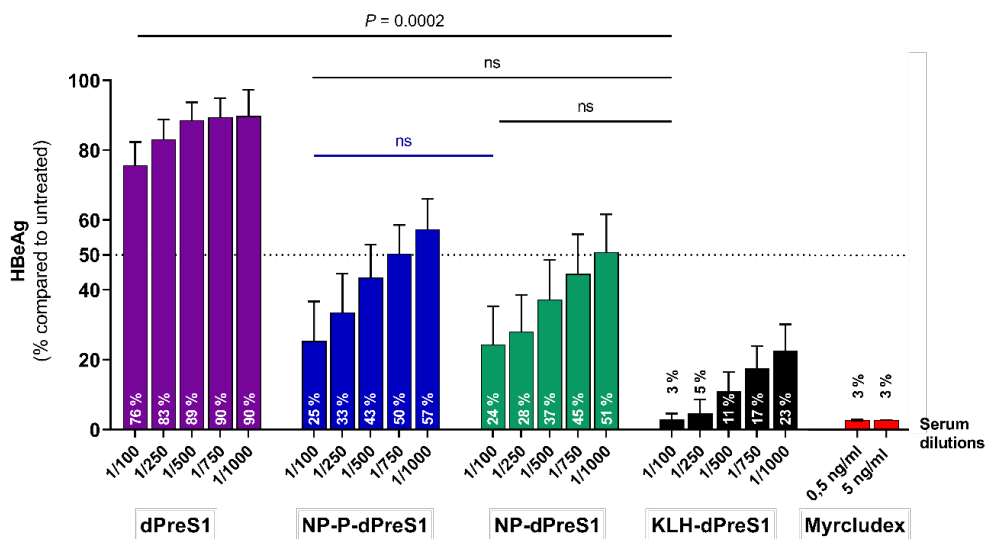
Fig. 6. Antibody response characterization. (A) Avidity indexes of anti-dPreS1 IgG were measured in mice sera at W6, W11, and W22. Antisera with index values exceeding 50% were attributed a high avidity, those with index values of 30% to 50% were attributed intermediate avidity, and those below to 30% were attributed a low avidity. Each symbol represents an individual animal and full bars indicate the mean of the group for each timepoint. **(B) IgG1 and IgG2a subtype titers were monitored in mice W13 and W22 sera.** Data are expressed in individual points with bars representing mean.

550
551
552

3.4. TLR2 agonist in the nanosystem generates strong neutralizing Ab

553
554
555
556
557
558
559
560
561
562

The *in vitro* neutralizing efficiency of the anti-dPreS1 Ab was investigated using infected differentiated HepaRG (dHepaRG) (Marion et al., 2010) and HBeAg was quantified as a parameter of viral infection establishment. While W11 sera from soluble dPreS1 immunization showed a weak neutralization effect (75% of HBeAg at 1/100 dilution), other groups induced strong neutralizing Ab against HBV, in a concentration-dependent manner (25%, 24% and 3% of HBeAg for respectively NP-P-dPreS1, NP-dPreS1 and KLH-dPreS1 at 1/100 dilution) (Fig. 7). W27 antisera was investigated similarly and HBV neutralization effect globally decreased (47%, 51% and 7% respectively for NP-P-dPreS1, NP-dPreS1 and KLH-dPreS1 groups). Immunization by soluble dPreS1 did not show any neutralization at W27, echoing the results from W11 (Fig. S5).

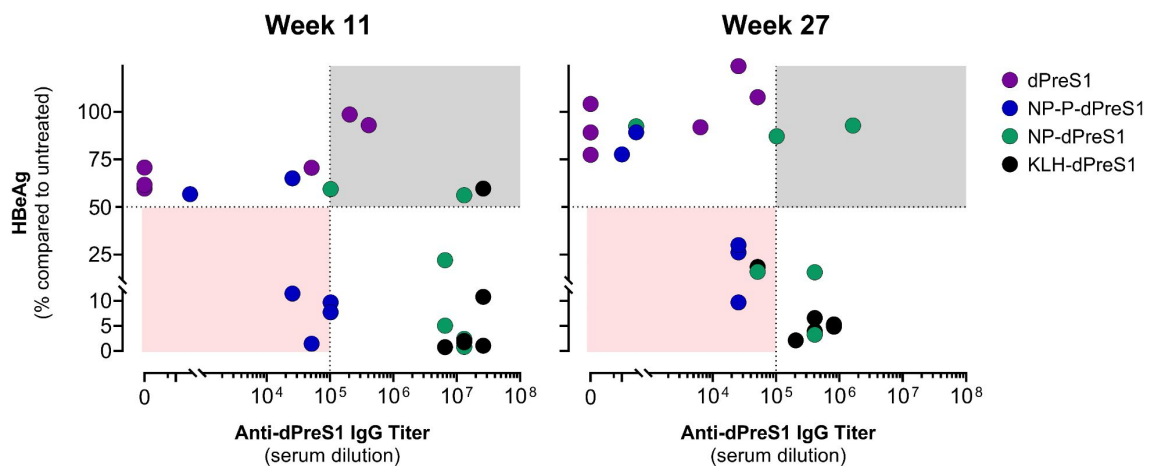


563
564
565

Fig. 7. *In vitro* HBV neutralization assay by murine anti-dPreS1 IgG from W11. Serum from W11 were serially diluted and incubated simultaneously with HBV on dHepaRG cell cultures (n=4),

566 washed the day after and then HBeAg concentrations were measured by ELISA after 7 days.
 567 Myrcludex, a polypeptide with HBV entry inhibitory properties, was use as positive control. Data is
 568 expressed as the percentage of HBeAg compared to non-treated (mean (SEM)). Two-way ANOVA
 569 was used for group comparisons (at 1/100 condition), with Dunnett's multiple comparison *post hoc*
 570 test for analysis of specific differences using either KLH-dPreS1 (black bars) or NP-dPreS1 (blue
 571 bar) as reference condition. $\alpha=0.05$.
 572

573 Surprisingly, the correlation of neutralizing data to the corresponding IgG titers suggests that
 574 Pam₃CSK₄ provides a distinct adjuvant-like effect to the immune response. At both W11 and 27,
 575 IgG from adjuvanted group showed a comparable neutralization profile as NP-dPreS1 IgG with
 576 100-fold lower Ab level (4/6 mice in the red squared area) (Fig. 8).
 577

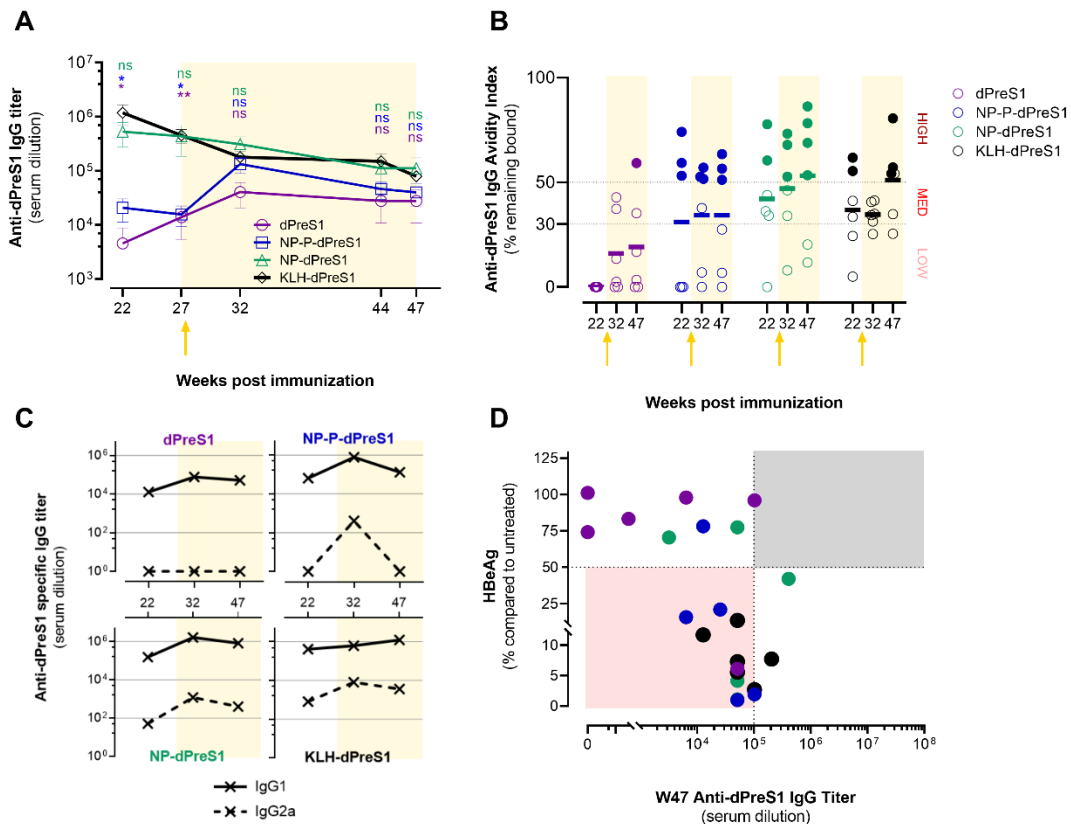


578
 579 **Fig. 8. Pam₃CSK₄ modulates the interactions between NP-dPreS1 and the immune system**
 580 **leading to IgG with the strongest neutralizing activity.** For each murine serum at W11 and 27,
 581 HBV neutralization activity (y axis) is represented according to the corresponding anti-dPreS1 IgG
 582 titer (x axis). Red squared areas highlight conditions with high neutralization power and low IgG
 583 titer, the most efficient combination. In contrast, gray squared areas highlight conditions with low
 584 neutralization power and high IgG titer. Data was gathered separately for easier visualization and
 585 each point represents one subject.
 586

587 3.5. Late heterologous boost confirms the essential role of nanovectorization for 588 immune benefit 589

590 The effect of a heterologous boost at W27 using the NP-dPreS1 candidate was investigated on
 591 NP-dPreS1 and NP-P-dPreS1 groups. Both received a s.c injection of NP-dPreS1 while control
 592 groups (KLH-dPreS1 and NP) received their respective formulations. The rationale was based on
 593 the literature suggesting that heterologous prime-boost can be more immunogenic than simple
 594 homologous strategy (Kardani et al., 2016; Lu, 2009). Concerning the soluble dPreS1 prime/NP-
 595 dPreS1 boost group (*purple data*), IgG titer and avidity index strongly increased without any effect
 596 in neutralization activity, confirming the crucial role of the prime immunization (Fig. 9A) (Havenar-
 597 Daughton et al., 2019). For the NP-P-dPreS1 prime/NP-dPreS1 boost group (*blue data*), we
 598 observed a similar increase of IgG titer and avidity index (Fig. 9B) with, more interestingly, a Th1
 599 cell polarization is induced with the emergence of IgG2a at W32 (Fig. 9D). The neutralization
 600 activity of these Ab is also greatly impacted with two-fold lower of HBeAg % level (from 46.5% at
 601 W27 to 23.5% at W47). Regarding NP-dPreS1 (*green data*) and KLH-dPreS1 (*black data*), they
 602 received their own homologous boost (to maintain the thoroughness of the controls), consolidating
 603 the strong existing immune response with highest avidity indexes changing from both medium to
 604 high levels. The neutralization level is higher for NP-dPreS1 (from 51.2% to 33.0%), while it is

605 unchanged for KLH-PreS1. Similar to the conventional prime-boost-boost regimen, NP-P-dPreS1
 606 group showed high neutralization efficiency while IgG titer is the lowest (*blue dots*), with 5/6 mice
 607 in the most efficient area (Fig. 9C).
 608



609 **Fig. 9. NP-dPreS1 s.c boost immunization on W27 improves the IgG titer and the**
 610 **neutralization effect (A)** Anti-dPreS1 IgG profiles from W22 to 47 with increase of titers for dPreS1
 611 and NP-P-dPreS1 formulations following final heterologous boost (*yellow arrow*). Data is expressed
 612 as mean (SD) and statistical analysis was performed by ANOVA test with multiple comparisons
 613 and Dunnett's correction using positive control KLH-dPreS1 condition as reference. $\alpha=0.05$,
 614 $*p<0.05$, $**p<0.005$, $***p<0.001$. **(B)** Avidity Index (%) after the final W27 boost also increases for
 615 all conditions. Full bars represent the mean for each condition. **(C)** Interestingly, IgG2a titers
 616 increase for nanoparticulate formulations (*blue and green*) but not for soluble dPreS1 (*purple*),
 617 following the final heterologous boost. **(D)** Neutralization effect compared to specific IgG titer at
 618 W47 hints at the added value of using a TLR adjuvant in therapy.
 619

620
 621 Concerning the toxicity profile of nanoformulations, the body weight of the mice was regularly
 622 monitored as well as the liver and spleen weights at the endpoint. Any general toxicity regarding
 623 these weights couldn't be detectable (Fig. S6). Further studies are intended to precisely describe
 624 the toxicological aspect, precisely the immunological consequence of a such treatment.
 625

626 4. Discussion

627
 628 In 2016, the World Health Organization stated the HBV elimination for 2030 as a global public
 629 health aim, by notably increasing the vaccine coverage from 82% to 90%. The development of
 630 novel vaccine technologies is thus crucial to reach it seeing as the current vaccine is sub-optimal
 631 (Block et al., 2021; Dolgin, 2022). Here, we have investigated the combination of a multivalent
 632 nanoplatform for an optimized Ag presentation with a TLR ligand entrapped in the delivery system
 633 to strengthen the neutralizing immune response. First, the nanosystem platform (PLA NP) is

634 synthesized by nanoprecipitation, an easy-to-use and industrially transposable process which
635 enables the production of reproducible and stable formulations. Second, an optimized antigenic
636 peptide, already used in clinical settings and derived from HBsAg, was adsorbed at the surface of
637 the NP. Lastly, since the induction of a strong and durable Ab response to vaccination is highly
638 dependent on the use of effective adjuvants that stimulates the innate immune system (Pulendran
639 and Ahmed, 2011), we chose to vectorize a TLR 1/2 agonist, Pam₃CSK₄ entrapped in the PLA NP
640 core to potentiate the immunization process.

641
642 In the first part of this study, straightforward molecular modeling results show that the choice of
643 Pam₃CSK₄ as the adjuvant and dPreS1 as the protein Ag is highly relevant in terms of chemical
644 mechanics. Indeed, both molecules do not interact with each other when formulated within the NP.
645 More precisely, vectorizing the antigen should be able to expose the dPreS1 epitopes, in presence
646 or not of Pam₃CSK₄, with no structural modification, and subsequently trigger identical
647 conformational Ab responses. This delivery system elegantly increases the immunogenicity and
648 stability of the Ag, by gathering it in nano-scale clusters and decreasing its risks of degradation.
649 Next, via crossed bioimaging and histological evaluations, we documented that an efficient entry of
650 vaccine into the lymphatic vessels can lead to an immune response by favoring the right timing and
651 right location in dLN. The biodistribution profile of fluorescent PLA nanosystems in mice show a
652 long-term stay in the secondary lymphoid organs, which is in favor of a slow and localized delivery
653 of the Ag. Interestingly, the adsorption of dPreS1 on the NP generates higher accumulation of the
654 vaccine in the draining areas but also facilitates the transport across tissues, leading to a greater
655 spatial diffusion over time. These data demonstrate that NP formulations have appropriate colloidal
656 and surface properties required for the dynamic process of immunization (Kelly et al., 2019).

657
658 Next, and despite initial delays in B cell activation and GC formation compared to controls, we
659 showed that the anti-PreS1 IgG titers and avidity indexes reached higher levels for the dually
660 functionalized formulation (NP-P-dPreS1). It is worth noting that both these read outs emphasize
661 the advantage of the nanovectorization on the bioavailability of the antigen and/or TLR1/2 adjuvant,
662 based on the intragroup response heterogeneity for the soluble dPreS1 compared to the NP groups
663 (Fig. S4). The increase in titers and avidity is in accordance with the general (Pedersen et al., 2020)
664 and the TLR-specific (DeFranco et al., 2012) literature, explaining the simultaneous but delayed
665 stimulation of both BCR and TLR signaling pathways. These findings also corroborates with past
666 papers indicating that activation of the TLR2-mediated NF-κB pathway in GC B cells controls GC
667 maintenance and differentiation (Heise et al., 2014). Desmares *et al* recently confirmed Pam₃CSK₄
668 specifically induced the activation of this canonical NF-κB pathway (Desmares et al., 2022).
669 Noteworthy, control groups (soluble Ag and NP) activated B cells after being taken in charge by
670 Ag-presenting cells but induced less GC formation and less or no IgG production. In parallel, we
671 report an elevation of serum CXCL13 levels during early immunization in presence of Pam₃CSK₄,
672 explained by the fact that CXCL13 expression occurred as a consequence of NF-κB activation
673 (Kazanietz et al., 2019). Altogether, these data are in favor of an enhanced spatiotemporal access
674 of the antigen and the adjuvant via their vectorization by the PLA NP.

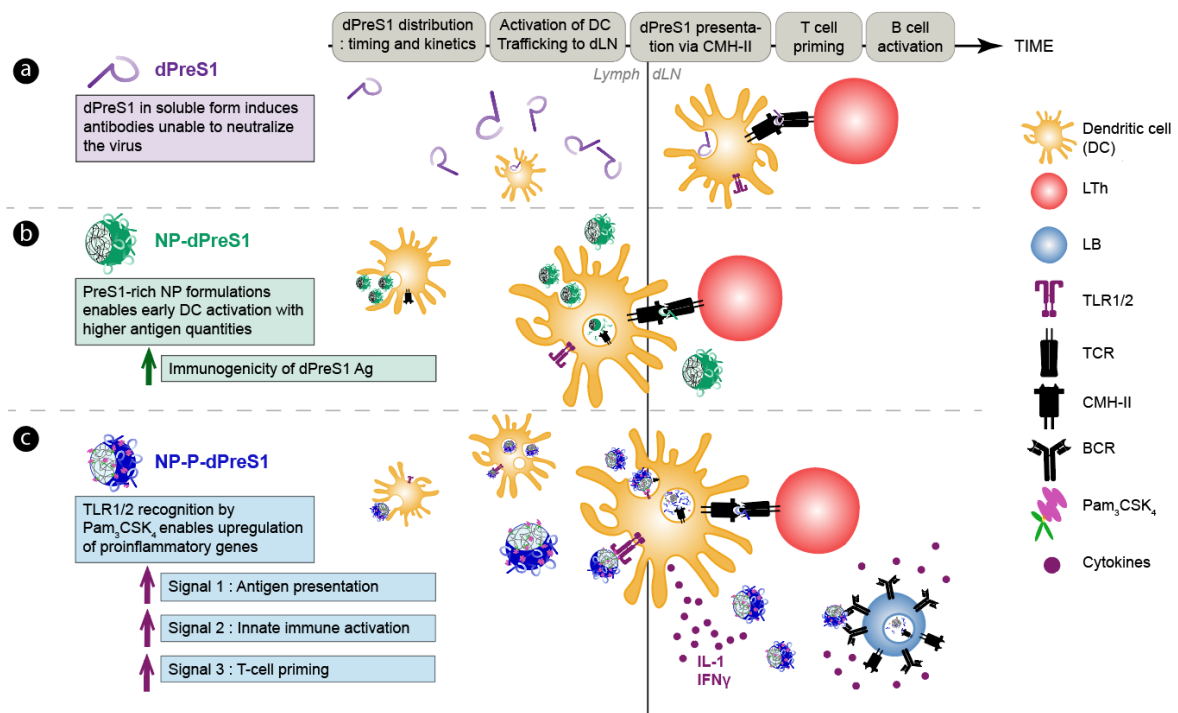
675
676 Subsequently, we confirmed the higher neutralizing capacity of vaccine-specific IgG when the Ag
677 is loaded onto NP versus the soluble form. Here again, in absence of a delivery system, the soluble
678 dPreS1 protein is rapidly exposed to proteolytic enzymes after subcutaneous administration which
679 impeded its presentation to the immune system (Varkhede et al., 2020). This observation validates
680 the previously established belief that drug drivers (Collins et al., 2017), such as NP (Kelly et al.,
681 2019), act as an efficient carrier for Ag transit, protection from the environment and presentation to
682 the lymphatic system. Likewise, vectorized dPreS1 is delivered to the LN for recognition and
683 internalization in higher-concentrated clusters, enhancing its immunogenicity (Kasturi et al., 2011).

684 Although there is no direct experimental explanation for this phenomenon yet, together with the MD
 685 data these findings prompted us to hypothesize that the doubly-functionalized NP has a synergistic
 686 effect between the adjuvant and the Ag and that the quality of the Ab prevails over their quantity.
 687 Future experiments are ongoing to verify this assumption.

688
 689 The neutralization data also show evidence of direct HBV entry inhibition in dHepaRG cells,
 690 indicating the Ab are effective at recognizing the 9-15 AA sequence of the viral surface protein and
 691 obstructing the PreS1/NTCP interaction (Urban et al., 2014). This observation reveals the diversity
 692 of B cell Ab-response to dPreS1 Ag in terms of immunoglobulin repertoire and neutralizing activity
 693 depending on the vaccine candidate. Next, we prove the added value of Pam₃CSK₄ adjuvant
 694 properties since mice immunized with NP entrapping this molecule led to greater humoral immune
 695 responses with higher virus-neutralizing Abs compared to NP formulated with dPreS1 only. The
 696 TLR1/2 ligand reinforces the quality of the immune response via the upregulation of
 697 proinflammatory genes subsequently leading to cytokine production and early B cell maturation
 698 improvement. Overall, NP-P-dPreS1 vaccine illustrates relevant preventive immunization
 699 properties. Again, after the heterologous boost, the presence of the adjuvant elicited the most
 700 interesting neutralizing activity of induced Ab with the highest neutralization efficiency adjusted to
 701 the IgG titers, and sustainable all over the year.

702
 703 We have summarized in Fig. 10 the current hypothesis regarding the immune key components
 704 responsible for triggering such optimal immune response when combining an adjuvant and a
 705 vaccine antigen onto the same polymeric particle. As one of the major challenges in vaccinology
 706 these days is to pin point which critical parameters of the innate immunity participates in the
 707 programming of the adaptive response, additional analyses of immune responses should be further
 708 characterized for full appreciation of the mechanism involved when using such nanoformulations.
 709 Typically, the enhanced quality of Ag produced could be studied by cloning and sequencing of B
 710 cell to identify Ab sequence with improved neutralizing properties.

711



712
 713
 714 **Fig. 10. Nanoadvantages and suggested immune mechanism triggered by soluble dPreS1**
 715 **versus adjuvanted or not NP-dPreS1 formulations. (a) Poor bioavailability of free-form soluble**
 716 **dPreS1 translates into suboptimal Ab production with late activation in dLNs of the immune cells.**

717 **(b)** LN trafficking and Ag immunogenicity: Nanovectorization gives rise to high-concentrated
718 clusters of dPreS1 Ag able to traffic longer in the lymphatics, two parameters that may explain an
719 enhanced immunogenicity of the Ag. **(c)** Innate immunity boost: TLR2 stimulus by Pam₃CSK₄ may
720 synergize with dPreS1 response and improve the GC pathway of memory B cell formation via three
721 different signals namely the enhancement of (i) the Ag presentation by DC, (ii) the innate immune
722 pro-inflammatory cytokines, and (iii) the subsequent T cell priming of HBV-specific CD4⁺ and
723 CD8⁺. In fact, the affinity selection of GC B cells is dependent on T cells (Pulendran, 2009).
724

725 Altogether, these results give high hopes for developing a successful therapeutic solution against
726 chronic HBV infections. Abundant efforts have been made to develop therapeutic vaccines but
727 most candidates have missed their primary endpoints, which may be attributed to the fact that they
728 have been composed of free Ag or micro-delivery systems, contributing to low uptake in the
729 lymphatics and failure to induce optimal protection (Kosinska et al., 2017; Li et al., 2017). With the
730 recent exception of two elegant studies, nearly no nanosystem solution has been explored (Qiao
731 et al., 2021; Wang et al., 2020). Qiao and colleagues propose a nanosystem based on chitosan
732 and heparin while Wang and colleagues developed a system based on ferritin NP. In terms of
733 biomaterials, chitosan is known to be very expensive and hard to produce in a reproducible manner,
734 while ferritin is a metallic-based system, which is less biocompatible and biodegradable than PLA
735 (Bellich et al., 2016). Nonetheless, mirroring our results, both these nanosystems display excellent
736 lymph node targeting following subcutaneous injections, as well as high IgG titers ($10^7 \log_{10}$ at week
737 7). Our novel subcutaneous delivery system could be part of the next generation antiviral
738 treatments for hepatitis patients, considering the long-lasting and highly specific immune protection
739 it triggers against PreS1 epitope. Strong tolerance to HBsAg have been shown to limit the
740 therapeutic effect of conventional vaccinations in both preclinical models and patients with chronic
741 hepatitis B infections. In the latter, immune tolerance to PreS1, if any, appears to be much lower
742 than that to HBsAg, as it is only secreted in trace amounts compared to HBsAg that is present in a
743 10^2 -fold to 10^5 -fold excess over virions (Durantel and Zoulim, 2016). Now, the formulation needs
744 to be challenged *in vivo* against HBV. This working hypothesis in AAV-HBV transduced mice is
745 currently undergoing. Such platforms are easily tunable and could quickly be adapted to any viral
746 genotype if the corresponding antigen is carefully selected. We could also imagine delivering both
747 the adjuvant and the Ag in separate PLA NP, offering flexibility in coupling a generic adjuvant-
748 containing NP with a novel antigen-containing NP (Boyoglu-Barnum et al., 2021; Singh et al., 2007).
749 Other nanoplatfoms can also be envisaged such as polymeric micelles already proved as efficient
750 adjuvants for vaccine delivery (Lamrayah et al., 2022).
751

752 Taking an even bigger step back, the precise characterization of this nanosystem participates in
753 broadening the R&D opportunities for hard-to-get microbes, such as HIV, *Plasmodium falciparum*,
754 or *Mycobacterium tuberculosis*. Incorporating such PLA NP in delivery systems like microneedle
755 platforms or hydrogels for high-mucus penetration would enable a better protection, with a mucosal-
756 specific immune activation at the localized site of entry of these pathogen (Du et al., 2022; Lavelle
757 and Ward, 2022).
758
759
760

761 **Conflict of interest**

762 All authors declare no conflict in interest except B.V. who holds some shares in Adjuvatis. The
763 company had no role in the design of the study; in the collection, analyses, or interpretation of data;
764 in the writing of the manuscript or in the decision to publish the results. The other authors declare
765 no conflict of interest.

766

767 **Authors contributions**

768 B.V., J.L. and D.D. conceived the idea, designed and supervised the work. M.L. and F.C. wrote the
769 original manuscript. S.M. and R.T. performed all in silico experiments. C.C., M.D. and D.D.
770 performed all in vitro experiments. E.C. performed all ex vivo experiments. M.L. and F.C. performed
771 all in vivo experiments. All authors have read, revised and agreed to the published version of the
772 manuscript.

773

774 **Acknowledgements**

775 The authors would like to thank the staff of AniCan platform (CRCL, Lyon) and Thomas Barré for
776 his assistance in FMT4000 equipment, PHENOCAN for imaging devices [grant number ANR-11-
777 EQPX-0035 PHENOCAN], all the staff of Plateau de Biologie Expérimentale de la Souris (ENS,
778 Lyon) for the generous advice with animal care, CT μ platform (Université Lyon 1) and Altan Yavuz
779 for electron microscopy assistance.

780

781 **Financial support**

782 This work was supported by “La Ligue contre le Cancer” to BV and DD and a PhD scholarship to
783 ML. This work was also supported by ANRS-MIE (French research agency on infectious and
784 emerging diseases) to BV and DD (ECTZ 62760 and ECTZ 160315) and through PhD scholarships
785 to FC (ECTZ158412) and MD (ECTZ137751). Global financial supports were also obtained from
786 CNRS and INSERM.

787 **Supplementary Data**

788

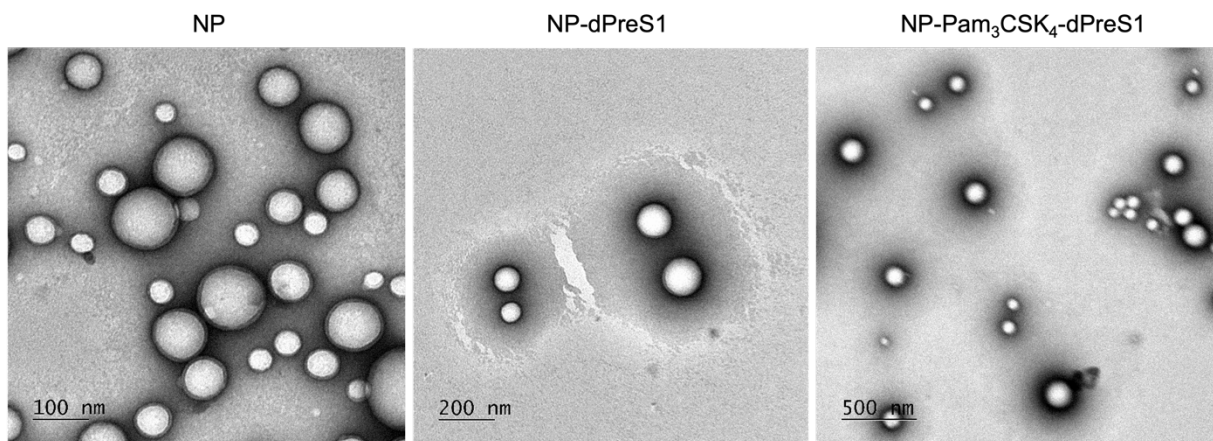
789 *Video attached to the manuscript*

790

791 **Video S1.** This video highlights the last 20 ns of the 200 ns simulation experiment. The last 1000
792 frames out of the 10,000 total frames of the dynamic were used. The simulation has reached a
793 stable state as no large molecular motion is observed. The biologically relevant epitope remains
794 accessible for intermolecular interactions throughout the complete capture. The epitope is
795 displayed in cyan, the lipidic anchor in yellow, and the rest of the PreS1 peptide in dark blue. PLA
796 chains are displayed in dark grey, red and light grey for their carbon, oxygen, and hydrogen atoms
797 respectively. The boundaries of the periodic cell are highlighted in dark green.

798

799



800

801 **Fig. S1. Transmission electron microscopy images of blank NP (left), NP-dPreS1 (center)**
802 **and NP-Pam₃CSK₄-dPreS1 (right).** The three types of nanoformulations are morphologically
803 similar (scale bar in each image).

804

805

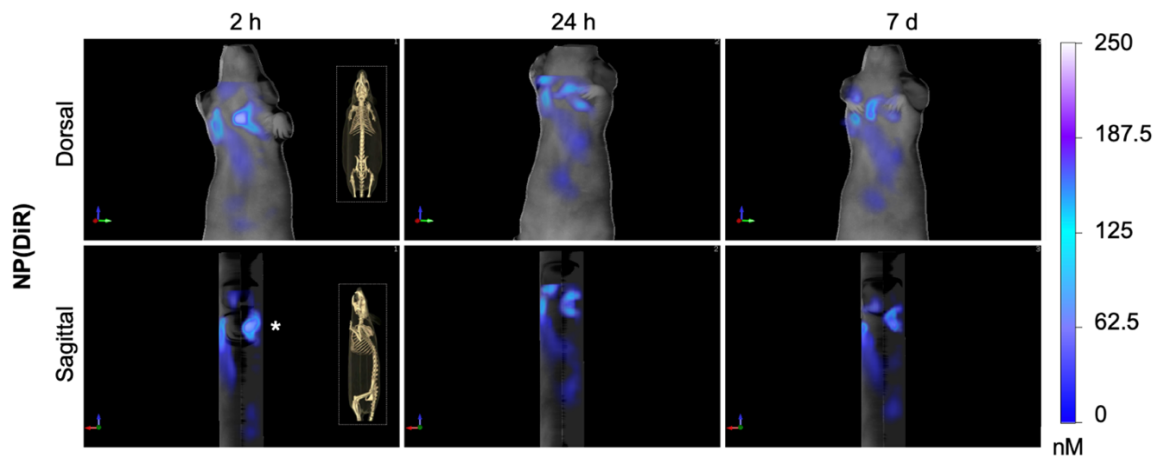
806 **A**

807

	Size (nm)	PDI	Zeta potential (mV)
NP(DiR)	160	0.078	-61
NP(DiR)-dPreS1	162	0.090	-64

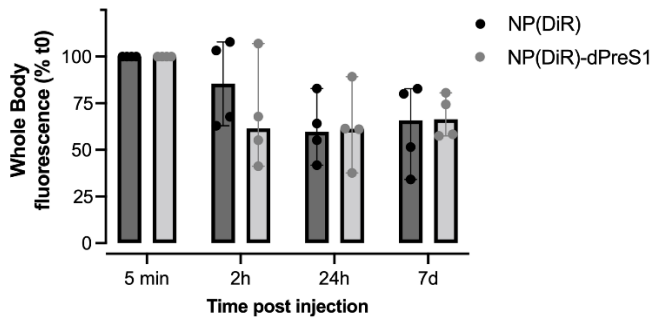
808

809 **B**



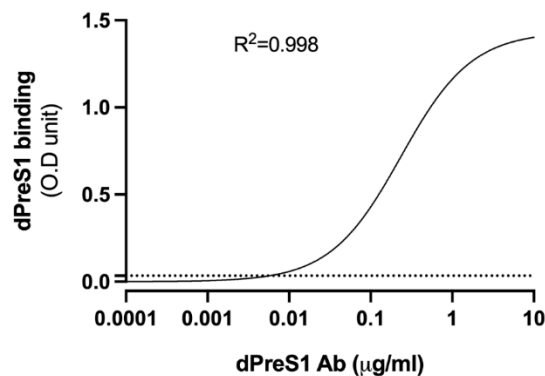
810
811

C



812
813

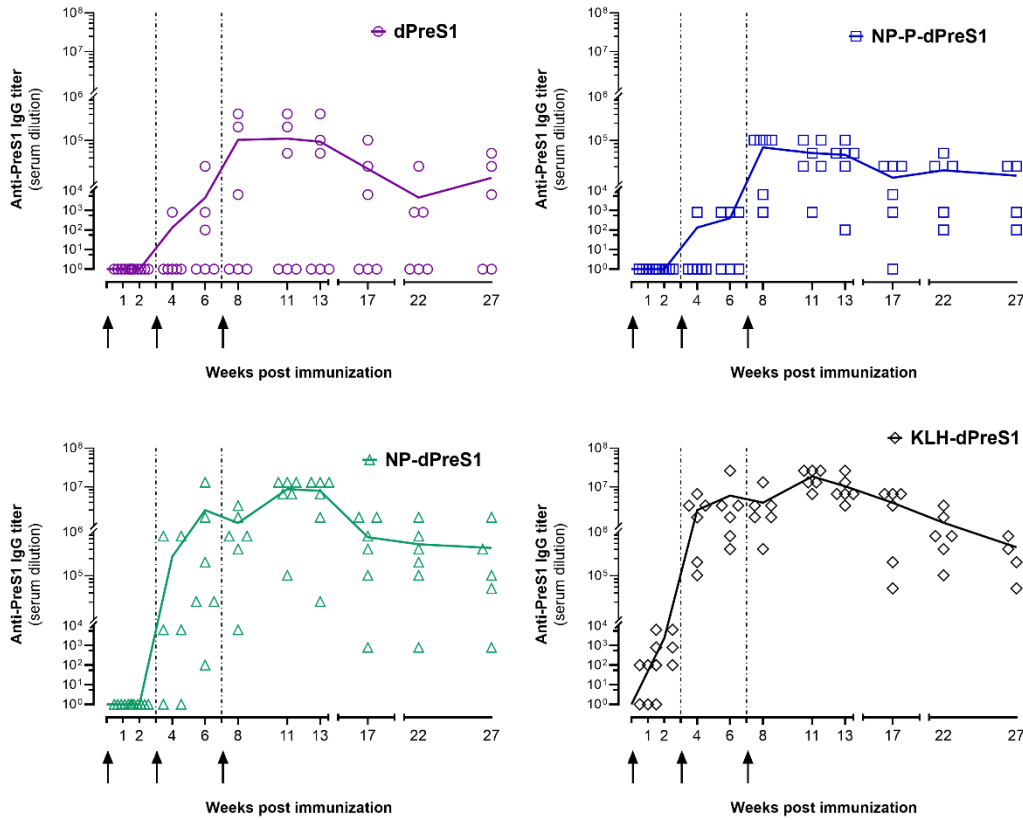
814 **Fig. S2. Comparative study of the biokinetics of the NP formulations functionalized or not**
 815 **with dPreS1. (A)** Standard colloidal properties of fluorescent formulations (size, PDI and surface
 816 charge) containing or not the modified dPreS1 peptide. **(B)** A single s.c injection (neck region, the
 817 injection site is shown by the asterisk) was performed on SKH1 female mice with fluorescent
 818 NP(DiR). The fluorescence intensity (750/780 nm) was monitored for 7 days using FMT imaging
 819 (Fluorescence Molecular Tomography, FMT4000, Perkin Elmer). **(C)** Fluorescence signal
 820 quantification measured by FMT in NP(DiR) or NP(DiR)-PreS1 injected mice, at different time
 821 points. Each point represents an individual animal and results are expressed as median (95% CI).
 822 Statistical differences between the two groups at each time were evaluated using the non-
 823 parametric Wilcoxon test. There is no statistical difference between the two fluorescence signals at
 824 each time.



825
826
827
828
829
830

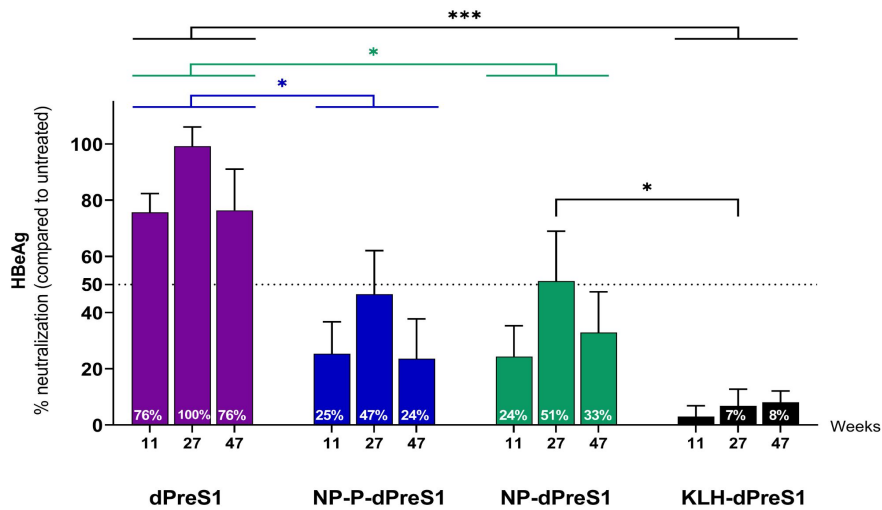
826 **Fig. S3. In-house sandwich ELISA for quantitative detection of specific dPreS1 Ab.** We have
 827 serially diluted a solution of anti-PreS1 Ab in dPreS1-coated plates. The limit of detection (LOD) is
 828 defined as $LOD = \mu \text{ blank} + 3\sigma$, and is represented by the dotted line.

831



832
833
834
835

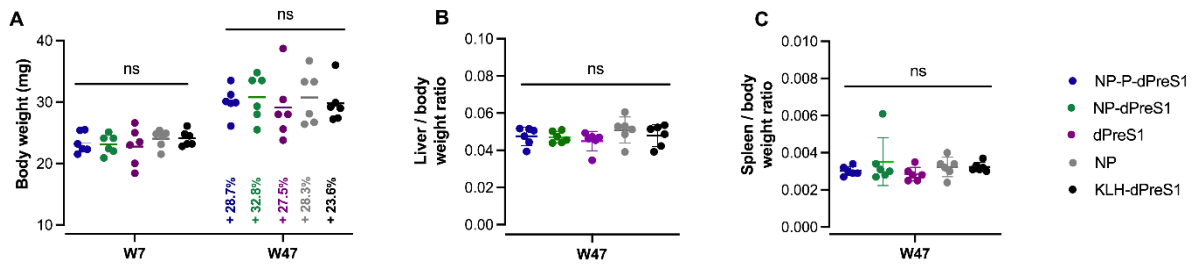
Fig. S4 IgG anti-dPreS1 titers, schematically represented in individual values. See legend of Figure 5



836

Fig. S5. Comparative data of the neutralization activity of mice antisera at W11, W27 and W47 in bar charts, at serum dilutions 1:100. Intragroup statistical analysis was performed by ANOVA test with multiple comparisons and Tukey's correction. For all groups, there was no intra-group difference ($\alpha = 0.05$) between the different time points.

841
842



843
844
845
846
847
848
849
850
851
852

Fig. S6. General safety evaluation based on weights is in favor of a safe-by-design nanoplatform. For toxicity surveillance, mice body weights were monitored at W7 and W47 with indicated each evolution rate (A). At endpoint, their liver (B) and spleen (C) were also weighed after cervical dislocation and dissection. Upon evaluation, no statistical difference was observed between groups (ANOVA test for A, Kruskal-Wallis test for B and C). Mice were physiologically heavier at one year old with an increasing weight between + 23.6% and + 32.8% compared to W7 weight. This information is important because toxicity can easily become a serious obstacle in the potential safety of a vaccine, especially when complemented by adjuvants. *ns* = *non significant*.

853 REFERENCES

854

- 855 Anwar, M.A., Shah, M., Kim, J., Choi, S., 2019. Recent clinical trends in Toll-like receptor
856 targeting therapeutics. *Med. Res. Rev.* 39, 1053–1090.
857 <https://doi.org/10.1002/med.21553>
- 858 Arulraj, T., Binder, S.C., Robert, P.A., Meyer-Hermann, M., 2019. Synchronous Germinal Center
859 Onset Impacts the Efficiency of Antibody Responses. *Front. Immunol.* 10.
860 <https://doi.org/10.3389/fimmu.2019.02116>
- 861 Badamchi-Zadeh, A., McKay, P.F., Korber, B.T., Barinaga, G., Walters, A.A., Nunes, A., Gomes,
862 J.P., Follmann, F., Tregoning, J.S., Shattock, R.J., 2016. A Multi-Component Prime-Boost
863 Vaccination Regimen with a Consensus MOMP Antigen Enhances Chlamydia
864 trachomatis Clearance. *Front. Immunol.* 7, 162. <https://doi.org/10.3389/fimmu.2016.00162>
- 865 Bellich, B., D'Agostino, I., Semeraro, S., Gamini, A., Cesàro, A., 2016. “The Good, the Bad and
866 the Ugly” of Chitosans. *Mar. Drugs* 14, 99. <https://doi.org/10.3390/md14050099>
- 867 Bian, Y., Zhang, Z., Sun, Z., Zhao, J., Zhu, D., Wang, Y., Fu, S., Guo, J., Liu, L., Su, L., Wang, F.-
868 S., Fu, Y.-X., Peng, H., 2017. Vaccines targeting preS1 domain overcome immune
869 tolerance in hepatitis B virus carrier mice. *Hepatology* 66, 1067–1082.
870 <https://doi.org/10.1002/hep.29239>
- 871 Block, T.M., Chang, K.-M., Guo, J.-T., 2021. Prospects for the Global Elimination of Hepatitis B.
872 *Annu. Rev. Virol.* 8, 437–458. <https://doi.org/10.1146/annurev-virology-091919-062728>
- 873 Boyoglu-Barnum, S., Ellis, D., Gillespie, R.A., Hutchinson, G.B., Park, Y.-J., Moin, S.M., Acton,
874 O.J., Ravichandran, R., Murphy, M., Pettie, D., Matheson, N., Carter, L., Creanga, A.,
875 Watson, M.J., Kephart, S., Ataca, S., Vaile, J.R., Ueda, G., Crank, M.C., Stewart, L., Lee,
876 K.K., Guttman, M., Baker, D., Mascola, J.R., Velesler, D., Graham, B.S., King, N.P.,
877 Kanekiyo, M., 2021. Quadrivalent influenza nanoparticle vaccines induce broad
878 protection. *Nature* 1–6. <https://doi.org/10.1038/s41586-021-03365-x>
- 879 Bray, F., Ferlay, J., Soerjomataram, I., Siegel, R.L., Torre, L.A., Jemal, A., 2018. Global cancer
880 statistics 2018: GLOBOCAN estimates of incidence and mortality worldwide for 36
881 cancers in 185 countries. *CA. Cancer J. Clin.* 68, 394–424.
882 <https://doi.org/10.3322/caac.21492>
- 883 Bretscher, P., 2019. On Analyzing How the Th1/Th2 Phenotype of an Immune Response Is
884 Determined: Classical Observations Must Not Be Ignored. *Front. Immunol.* 10.
885 <https://doi.org/10.3389/fimmu.2019.01234>
- 886 Brisse, M., Vrba, S.M., Kirk, N., Liang, Y., Ly, H., 2020. Emerging Concepts and Technologies in
887 Vaccine Development. *Front. Immunol.* 11, 583077.
888 <https://doi.org/10.3389/fimmu.2020.583077>
- 889 Chaudhury, S., Gray, J.J., 2008. Conformer Selection and Induced Fit in Flexible Backbone
890 Protein–Protein Docking Using Computational and NMR Ensembles. *J. Mol. Biol.* 381,
891 1068–1087. <https://doi.org/10.1016/j.jmb.2008.05.042>
- 892 Cheng, D., Han, B., Zhang, W., Wu, W., 2021. Clinical effects of NTCP-inhibitor myrcludex B. *J.*
893 *Viral Hepat.* 28, 852–858. <https://doi.org/10.1111/jvh.13490>
- 894 ClusPro 2.0: protein-protein docking [WWW Document], n.d. URL <https://cluspro.org/login.php>
895 (accessed 7.19.21).
- 896 Collins, D.S., Kourtis, L.C., Thyagarajapuram, N.R., Sirkar, R., Kapur, S., Harrison, M.W., Bryan,
897 D.J., Jones, G.B., Wright, J.M., 2017. Optimizing the Bioavailability of Subcutaneously
898 Administered Biotherapeutics Through Mechanochemical Drivers. *Pharm. Res.* 34, 2000–
899 2011. <https://doi.org/10.1007/s11095-017-2229-9>
- 900 Coolen, A.-L., Lacroix, C., Mercier-Gouy, P., Delaune, E., Monge, C., Exposito, J.-Y., Verrier, B.,
901 2019. Poly(lactic acid) nanoparticles and cell-penetrating peptide potentiate mRNA-based
902 vaccine expression in dendritic cells triggering their activation. *Biomaterials* 195, 23–37.
903 <https://doi.org/10.1016/j.biomaterials.2018.12.019>
- 904 Dalzon, B., Lebas, C., Jimenez, G., Gutjahr, A., Terrat, C., Exposito, J.-Y., Verrier, B., Lethias, C.,
905 2016. Poly(Lactic Acid) Nanoparticles Targeting $\alpha 5\beta 1$ Integrin as Vaccine Delivery
906 Vehicle, a Prospective Study. *PloS One* 11, e0167663.
907 <https://doi.org/10.1371/journal.pone.0167663>
- 908 De Silva, N.S., Klein, U., 2015. Dynamics of B cells in germinal centres. *Nat. Rev. Immunol.* 15,
909 137–148. <https://doi.org/10.1038/nri3804>

- 910 DeFranco, A.L., Rookhuizen, D.C., Hou, B., 2012. Contribution of TLR signaling to germinal
911 center antibody responses. *Immunol. Rev.* 247, 64–72. [https://doi.org/10.1111/j.1600-](https://doi.org/10.1111/j.1600-065X.2012.01115.x)
912 065X.2012.01115.x
- 913 Dembek, C., Protzer, U., Roggendorf, M., 2018. Overcoming immune tolerance in chronic
914 hepatitis B by therapeutic vaccination. *Curr. Opin. Virol.* 30, 58–67.
915 <https://doi.org/10.1016/j.coviro.2018.04.003>
- 916 Desmares, M., Delphin, M., Chardès, B., Pons, C., Riedinger, J., Michelet, M., Rivoire, M.,
917 Verrier, B., Salvetti, A., Lucifora, J., Durantel, D., 2022. Insights on the antiviral
918 mechanisms of action of the TLR1/2 agonist Pam3CSK4 in hepatitis B virus (HBV)-
919 infected hepatocytes. *Antiviral Res.* 206, 105386.
920 <https://doi.org/10.1016/j.antiviral.2022.105386>
- 921 Dolgin, E., 2022. Closing in on a cure for hepatitis B. *Nature* 603, S46–S48.
922 <https://doi.org/10.1038/d41586-022-00812-1>
- 923 Dou, Y., Jansen, D.T.S.L., van den Bosch, A., de Man, R.A., van Montfoort, N., Araman, C., van
924 Kasteren, S.I., Zom, G.G., Krebber, W.-J., Melief, C.J.M., Woltman, A.M., Buschow, S.I.,
925 2020. Design of TLR2-ligand-synthetic long peptide conjugates for therapeutic
926 vaccination of chronic HBV patients. *Antiviral Res.* 178, 104746.
927 <https://doi.org/10.1016/j.antiviral.2020.104746>
- 928 Du, G., Qin, M., Sun, X., 2022. Recent progress in application of nanovaccines for enhancing
929 mucosal immune responses. *Acta Pharm. Sin. B.*
930 <https://doi.org/10.1016/j.apsb.2022.08.010>
- 931 Durantel, D., Zoulim, F., 2016. New antiviral targets for innovative treatment concepts for hepatitis
932 B virus and hepatitis delta virus. *J. Hepatol., Molecular Biology of Hepatitis B Virus* 64,
933 S117–S131. <https://doi.org/10.1016/j.jhep.2016.02.016>
- 934 Fanning, G.C., Zoulim, F., Hou, J., Bertoletti, A., 2019. Therapeutic strategies for hepatitis B virus
935 infection: towards a cure. *Nat. Rev. Drug Discov.* 18, 827–844.
936 <https://doi.org/10.1038/s41573-019-0037-0>
- 937 Fries, C.N., Curvino, E.J., Chen, J.-L., Permar, S.R., Fouda, G.G., Collier, J.H., 2020. Advances
938 in nanomaterial vaccine strategies to address infectious diseases impacting global health.
939 *Nat. Nanotechnol.* <https://doi.org/10.1038/s41565-020-0739-9>
- 940 Glebe, D., Urban, S., Knoop, E.V., Cag, N., Krass, P., Grün, S., Bulavaite, A., Sasnauskas, K.,
941 Gerlich, W.H., 2005. Mapping of the hepatitis B virus attachment site by use of infection-
942 inhibiting preS1 lipopeptides and tupaia hepatocytes. *Gastroenterology* 129, 234–245.
943 <https://doi.org/10.1053/j.gastro.2005.03.090>
- 944 Graber-Stiehl, I., 2018. The silent epidemic killing more people than HIV, malaria or TB. *Nature*
945 564, 24–26. <https://doi.org/10.1038/d41586-018-07592-7>
- 946 Gripon, P., Rumin, S., Urban, S., Le Seyec, J., Glaise, D., Cannie, I., Guyomard, C., Lucas, J.,
947 Trepo, C., Guguen-Guillouzo, C., 2002. Infection of a human hepatoma cell line by
948 hepatitis B virus. *Proc. Natl. Acad. Sci. U. S. A.* 99, 15655–15660.
949 <https://doi.org/10.1073/pnas.232137699>
- 950 Gutjahr, A., Phelip, C., Coolen, A.-L., Monge, C., Boisgard, A.-S., Paul, S., Verrier, B., 2016.
951 Biodegradable Polymeric Nanoparticles-Based Vaccine Adjuvants for Lymph Nodes
952 Targeting. *Vaccines* 4. <https://doi.org/10.3390/vaccines4040034>
- 953 Harris, J.R., Markl, J., 1999. Keyhole limpet hemocyanin (KLH): a biomedical review. *Micron* 30,
954 597–623. [https://doi.org/10.1016/S0968-4328\(99\)00036-0](https://doi.org/10.1016/S0968-4328(99)00036-0)
- 955 Havenar-Daughton, C., Carnathan, D.G., Boopathy, A.V., Upadhyay, A.A., Murrell, B., Reiss,
956 S.M., Enemu, C.A., Gebru, E.H., Choe, Y., Dhadvai, P., Viviano, F., Kaushik, K.,
957 Bhiman, J.N., Briney, B., Burton, D.R., Bosinger, S.E., Schief, W.R., Irvine, D.J., Silvestri,
958 G., Crotty, S., 2019. Rapid Germinal Center and Antibody Responses in Non-human
959 Primates after a Single Nanoparticle Vaccine Immunization 35.
- 960 Havenar-Daughton, C., Lindqvist, M., Heit, A., Wu, J.E., Reiss, S.M., Kendric, K., Bélanger, S.,
961 Kasturi, S.P., Landais, E., Akondy, R.S., McGuire, H.M., Bothwell, M., Vagefi, P.A.,
962 Scully, E., Tomaras, G.D., Davis, M.M., Pognard, P., Ahmed, R., Walker, B.D.,
963 Pulendran, B., McElrath, M.J., Kaufmann, D.E., Crotty, S., 2016. CXCL13 is a plasma
964 biomarker of germinal center activity. *Proc. Natl. Acad. Sci. U. S. A.* 113, 2702–2707.
965 <https://doi.org/10.1073/pnas.1520112113>
- 966 Heise, N., De Silva, N.S., Silva, K., Carette, A., Simonetti, G., Pasparakis, M., Klein, U., 2014.
967 Germinal center B cell maintenance and differentiation are controlled by distinct NF-κB

968 transcription factor subunits. *J. Exp. Med.* 211, 2103–2118.
969 <https://doi.org/10.1084/jem.20132613>

970 Hennessy, E.J., Parker, A.E., O'Neill, L.A.J., 2010. Targeting Toll-like receptors: emerging
971 therapeutics? *Nat. Rev. Drug Discov.* 9, 293–307. <https://doi.org/10.1038/nrd3203>

972 I-TASSER server for protein structure and function prediction [WWW Document], n.d. URL
973 <https://zhanglab.ccmb.med.umich.edu/I-TASSER/> (accessed 12.6.19).

974 Kardani, K., Bolhassani, A., Shahbazi, S., 2016. Prime-boost vaccine strategy against viral
975 infections: Mechanisms and benefits. *Vaccine* 34, 413–423.
976 <https://doi.org/10.1016/j.vaccine.2015.11.062>

977 Kasturi, S.P., Skountzou, I., Albrecht, R.A., Koutsouanos, D., Hua, T., Nakaya, H.I., Ravindran,
978 R., Stewart, S., Alam, M., Kwissa, M., Villinger, F., Murthy, N., Steel, J., Jacob, J., Hogan,
979 R.J., García-Sastre, A., Compans, R., Pulendran, B., 2011. Programming the magnitude
980 and persistence of antibody responses with innate immunity. *Nature* 470, 543–547.
981 <https://doi.org/10.1038/nature09737>

982 Kazanietz, M.G., Durando, M., Cooke, M., 2019. CXCL13 and Its Receptor CXCR5 in Cancer:
983 Inflammation, Immune Response, and Beyond. *Front. Endocrinol.* 10.
984 <https://doi.org/10.3389/fendo.2019.00471>

985 Kelly, H.G., Kent, S.J., Wheatley, A.K., 2019. Immunological basis for enhanced immunity of
986 nanoparticle vaccines. *Expert Rev. Vaccines* 18, 269–280.
987 <https://doi.org/10.1080/14760584.2019.1578216>

988 Kosinska, A.D., Bauer, T., Protzer, U., 2017. Therapeutic vaccination for chronic hepatitis B. *Curr.*
989 *Opin. Virol., Viral pathogenesis • Preventive and therapeutic vaccines* 23, 75–81.
990 <https://doi.org/10.1016/j.coviro.2017.03.011>

991 Lamalle-Bernard, D., Munier, S., Compagnon, C., Charles, M.-H., Kalyanaraman, V.S., Delair, T.,
992 Verrier, B., Ataman-Onal, Y., 2006. Coadsorption of HIV-1 p24 and gp120 proteins to
993 surfactant-free anionic PLA nanoparticles preserves antigenicity and immunogenicity. *J.*
994 *Control. Release Off. J. Control. Release Soc.* 115, 57–67.
995 <https://doi.org/10.1016/j.jconrel.2006.07.006>

996 Lamrayah, M., Charriaud, F., Hu, S., Megy, S., Terreux, R., Verrier, B., 2019. Molecular modelling
997 of TLR agonist Pam3CSK4 entrapment in PLA nanoparticles as a tool to explain loading
998 efficiency and functionality. *Int. J. Pharm.* 568, 118569.
999 <https://doi.org/10.1016/j.ijpharm.2019.118569>

1000 Lamrayah, M., Phelip, C., Coiffier, C., Lacroix, C., Willemin, T., Trimaille, T., Verrier, B., 2022. A
1001 Polylactide-Based Micellar Adjuvant Improves the Intensity and Quality of Immune
1002 Response. *Pharmaceutics* 14, 107. <https://doi.org/10.3390/pharmaceutics14010107>

1003 Lang, J., Neumann-Haefelin, C., Thimme, R., 2019. Immunological cure of HBV infection.
1004 *Hepatol. Int.* 13, 113–124. <https://doi.org/10.1007/s12072-018-9912-8>

1005 Lavelle, E.C., Ward, R.W., 2022. Mucosal vaccines — fortifying the frontiers. *Nat. Rev. Immunol.*
1006 22, 236–250. <https://doi.org/10.1038/s41577-021-00583-2>

1007 Lee, G.-H., Lim, S.-G., 2021. CpG-Adjuvanted Hepatitis B Vaccine (HEPLISAV-B®) Update.
1008 *Expert Rev. Vaccines* 20, 487–495. <https://doi.org/10.1080/14760584.2021.1908133>

1009 Lee, S.-H., Park, S.-R., 2018. Toll-like Receptor 1/2 Agonist Pam3CSK4 Suppresses
1010 Lipopolysaccharide-driven IgG1 Production while Enhancing IgG2a Production by B
1011 Cells. *Immune Netw.* 18. <https://doi.org/10.4110/in.2018.18.e10>

1012 Li, J., Bao, M., Ge, J., Ren, S., Zhou, T., Qi, F., Pu, X., Dou, J., 2017. Research progress of
1013 therapeutic vaccines for treating chronic hepatitis B. *Hum. Vaccines Immunother.* 13,
1014 986–997. <https://doi.org/10.1080/21645515.2016.1276125>

1015 Lu, S., 2009. Heterologous prime-boost vaccination. *Curr. Opin. Immunol.* 21, 346–351.
1016 <https://doi.org/10.1016/j.coi.2009.05.016>

1017 Lucifora, J., Bonnin, M., Aillot, L., Fusil, F., Maadadi, S., Dimier, L., Michelet, M., Floriot, O.,
1018 Ollivier, A., Rivoire, M., Ait-Goughoulte, M., Daffis, S., Fletcher, S.P., Salvetti, A., Cosset,
1019 F.-L., Zoulim, F., Durantel, D., 2018. Direct antiviral properties of TLR ligands against
1020 HBV replication in immune-competent hepatocytes. *Sci. Rep.* 8, 5390.
1021 <https://doi.org/10.1038/s41598-018-23525-w>

1022 Marion, M.-J., Hantz, O., Durantel, D., 2010. The HepaRG Cell Line: Biological Properties and
1023 Relevance as a Tool for Cell Biology, Drug Metabolism, and Virology Studies, in: Maurel,
1024 P. (Ed.), *Hepatocytes: Methods and Protocols, Methods in Molecular Biology*. Humana
1025 Press, Totowa, NJ, pp. 261–272. https://doi.org/10.1007/978-1-60761-688-7_13

1026 Megy, S., Agüero, S., Da Costa, D., Lamrayah, M., Berthet, M., Primard, C., Verrier, B., Terreux,
1027 R., 2020. Molecular Dynamics Studies of Poly(Lactic Acid) Nanoparticles and Their
1028 Interactions with Vitamin E and TLR Agonists Pam1CSK4 and Pam3CSK4.
1029 *Nanomaterials* 10, 2209. <https://doi.org/10.3390/nano10112209>

1030 Meier, A., Mehrle, S., Weiss, T.S., Mier, W., Urban, S., 2013. Myristoylated PreS1-domain of the
1031 hepatitis B virus L-protein mediates specific binding to differentiated hepatocytes.
1032 *Hepatology* 58, 31–42. <https://doi.org/10.1002/hep.26181>

1033 Meng, Z., Chen, Y., Lu, M., 2019. Advances in Targeting the Innate and Adaptive Immune
1034 Systems to Cure Chronic Hepatitis B Virus Infection. *Front. Immunol.* 10, 3127.
1035 <https://doi.org/10.3389/fimmu.2019.03127>

1036 Mitchell, M.J., Billingsley, M.M., Haley, R.M., Wechsler, M.E., Peppas, N.A., Langer, R., 2020.
1037 Engineering precision nanoparticles for drug delivery. *Nat. Rev. Drug Discov.* 1–24.
1038 <https://doi.org/10.1038/s41573-020-0090-8>

1039 Monrad, J.T., Sandbrink, J.B., Cherian, N.G., 2021. Promoting versatile vaccine development for
1040 emerging pandemics. *Npj Vaccines* 6, 1–7. <https://doi.org/10.1038/s41541-021-00290-y>

1041 Ni, Y., Lempp, F.A., Mehrle, S., Nkongolo, S., Kaufman, C., Fälth, M., Stindt, J., Königer, C.,
1042 Nassal, M., Kubitz, R., Sülthmann, H., Urban, S., 2014. Hepatitis B and D viruses exploit
1043 sodium taurocholate co-transporting polypeptide for species-specific entry into
1044 hepatocytes. *Gastroenterology* 146, 1070–1083.
1045 <https://doi.org/10.1053/j.gastro.2013.12.024>

1046 Park, H., Bradley, P., Greisen, P., Liu, Y., Mulligan, V.K., Kim, D.E., Baker, D., DiMaio, F., 2016.
1047 Simultaneous Optimization of Biomolecular Energy Functions on Features from Small
1048 Molecules and Macromolecules. *J. Chem. Theory Comput.* 12, 6201–6212.
1049 <https://doi.org/10.1021/acs.jctc.6b00819>

1050 Pavot, V., Climent, N., Rochereau, N., Garcia, F., Genin, C., Tiraby, G., Vernejoul, F., Perouzel,
1051 E., Lioux, T., Verrier, B., Paul, S., 2016. Directing vaccine immune responses to mucosa
1052 by nanosized particulate carriers encapsulating NOD ligands. *Biomaterials* 75, 327–339.
1053 <https://doi.org/10.1016/j.biomaterials.2015.10.034>

1054 Pavot, V., Rochereau, N., Primard, C., Genin, C., Perouzel, E., Lioux, T., Paul, S., Verrier, B.,
1055 2013. Encapsulation of Nod1 and Nod2 receptor ligands into poly(lactic acid)
1056 nanoparticles potentiates their immune properties. *J. Control. Release Off. J. Control.*
1057 *Release Soc.* 167, 60–67. <https://doi.org/10.1016/j.jconrel.2013.01.015>

1058 Pedersen, G.K., Wørzner, K., Andersen, P., Christensen, D., 2020. Vaccine Adjuvants
1059 Differentially Affect Kinetics of Antibody and Germinal Center Responses. *Front.*
1060 *Immunol.* 11. <https://doi.org/10.3389/fimmu.2020.579761>

1061 Peplow, M., 2021. Nanotechnology offers alternative ways to fight COVID-19 pandemic with
1062 antivirals. *Nat. Biotechnol.* 39, 1172–1174. <https://doi.org/10.1038/s41587-021-01085-1>

1063 Peres, C., Matos, A.I., Connot, J., Sainz, V., Zupančič, E., Silva, J.M., Graça, L., Sá Gaspar, R.,
1064 Prêat, V., Florindo, H.F., 2017. Poly(lactic acid)-based particulate systems are promising
1065 tools for immune modulation. *Acta Biomater.* 48, 41–57.
1066 <https://doi.org/10.1016/j.actbio.2016.11.012>

1067 Polaris Observatory Collaborators, 2018. Global prevalence, treatment, and prevention of
1068 hepatitis B virus infection in 2016: a modelling study. *Lancet Gastroenterol. Hepatol.* 3,
1069 383–403. [https://doi.org/10.1016/S2468-1253\(18\)30056-6](https://doi.org/10.1016/S2468-1253(18)30056-6)

1070 Pulendran, B., 2009. Learning immunology from the yellow fever vaccine: innate immunity to
1071 systems vaccinology. *Nat. Rev. Immunol.* 9, 741–747. <https://doi.org/10.1038/nri2629>

1072 Pulendran, B., Ahmed, R., 2011. Immunological mechanisms of vaccination. *Nat. Immunol.* 12,
1073 509–517. <https://doi.org/10.1038/ni.2039>

1074 Pulendran, B., S. Arunachalam, P., O'Hagan, D.T., 2021. Emerging concepts in the science of
1075 vaccine adjuvants. *Nat. Rev. Drug Discov.* 1–22. <https://doi.org/10.1038/s41573-021-00163-y>

1076

1077 Qiao, D., Chen, Y., Liu, L., 2021. Engineered therapeutic nanovaccine against chronic hepatitis B
1078 virus infection. *Biomaterials* 269, 120674.
1079 <https://doi.org/10.1016/j.biomaterials.2021.120674>

1080 Qin, Y., Liao, P., 2018. Hepatitis B virus vaccine breakthrough infection: surveillance of S gene
1081 mutants of HBV. *Acta Virol.* 62, 115–121. https://doi.org/10.4149/av_2018_210

1082 Rammensee, H.-G., Wiesmüller, K.-H., Chandran, P.A., Zelba, H., Rusch, E., Gouttefangeas, C.,
1083 Kowalewski, D.J., Di Marco, M., Haen, S.P., Walz, J.S., Gloria, Y.C., Bödder, J., Schertel,
1084 J.-M., Tunger, A., Müller, L., Kießler, M., Wehner, R., Schmitz, M., Jakobi, M.,

1085 Schneiderhan-Marra, N., Klein, R., Laske, K., Artzner, K., Backert, L., Schuster, H.,
1086 Schwenck, J., Weber, A.N.R., Pichler, B.J., Kneilling, M., la Fougère, C., Forchhammer,
1087 S., Metzler, G., Bauer, J., Weide, B., Schippert, W., Stevanović, S., Löffler, M.W., 2019. A
1088 new synthetic toll-like receptor 1/2 ligand is an efficient adjuvant for peptide vaccination in
1089 a human volunteer. *J. Immunother. Cancer* 7, 307. [https://doi.org/10.1186/s40425-019-](https://doi.org/10.1186/s40425-019-0796-5)
1090 [0796-5](https://doi.org/10.1186/s40425-019-0796-5)

1091 Rességuier, J., Delaune, E., Coolen, A.-L., Levraud, J.-P., Boudinot, P., Le Guellec, D., Verrier,
1092 B., 2017. Specific and Efficient Uptake of Surfactant-Free Poly(Lactic Acid) Nanovaccine
1093 Vehicles by Mucosal Dendritic Cells in Adult Zebrafish after Bath Immersion. *Front.*
1094 *Immunol.* 8, 190. <https://doi.org/10.3389/fimmu.2017.00190>

1095 Saco, T.V., Strauss, A.T., Ledford, D.K., 2018. Hepatitis B vaccine nonresponders: Possible
1096 mechanisms and solutions. *Ann. Allergy Asthma Immunol. Off. Publ. Am. Coll. Allergy*
1097 *Asthma Immunol.* 121, 320–327. <https://doi.org/10.1016/j.anai.2018.03.017>

1098 Schudel, A., Francis, D.M., Thomas, S.N., 2019. Material design for lymph node drug delivery.
1099 *Nat. Rev. Mater.* 4, 415–428. <https://doi.org/10.1038/s41578-019-0110-7>

1100 Singh, A., 2021. Eliciting B cell immunity against infectious diseases using nanovaccines. *Nat.*
1101 *Nanotechnol.* 16, 9.

1102 Singh, M., Chakrapani, A., O'Hagan, D., 2007. Nanoparticles and microparticles as vaccine-
1103 delivery systems. *Expert Rev. Vaccines* 6, 797–808.
1104 <https://doi.org/10.1586/14760584.6.5.797>

1105 Swaminathan, A., Lucas, R.M., Dear, K., McMichael, A.J., 2014. Keyhole limpet haemocyanin - a
1106 model antigen for human immunotoxicological studies. *Br. J. Clin. Pharmacol.* 78, 1135–
1107 1142. <https://doi.org/10.1111/bcp.12422>

1108 Urban, S., Bartenschlager, R., Kubitz, R., Zoulim, F., 2014. Strategies to inhibit entry of HBV and
1109 HDV into hepatocytes. *Gastroenterology* 147, 48–64.
1110 <https://doi.org/10.1053/j.gastro.2014.04.030>

1111 van Zundert, G.C.P., Rodrigues, J.P.G.L.M., Trellet, M., Schmitz, C., Kastiris, P.L., Karaca, E.,
1112 Melquiond, A.S.J., van Dijk, M., de Vries, S.J., Bonvin, A.M.J.J., 2016. The HADDOCK2.2
1113 Web Server: User-Friendly Integrative Modeling of Biomolecular Complexes. *J. Mol. Biol.*
1114 428, 720–725. <https://doi.org/10.1016/j.jmb.2015.09.014>

1115 Varkhede, N., Bommana, R., Schöneich, C., Forrest, M.L., 2020. Proteolysis and Oxidation of
1116 Therapeutic Proteins After Intradermal or Subcutaneous Administration. *J. Pharm. Sci.*
1117 109, 191–205. <https://doi.org/10.1016/j.xphs.2019.08.005>

1118 Victora, G.D., Nussenzweig, M.C., 2012. Germinal Centers. *Annu. Rev. Immunol.* 30, 429–457.
1119 <https://doi.org/10.1146/annurev-immunol-020711-075032>

1120 Wang, W., Zhou, X., Bian, Y., Wang, S., Chai, Q., Guo, Z., Wang, Z., Zhu, P., Peng, H., Yan, X.,
1121 Li, W., Fu, Y.-X., Zhu, M., 2020. Dual-targeting nanoparticle vaccine elicits a therapeutic
1122 antibody response against chronic hepatitis B. *Nat. Nanotechnol.* 15, 406–416.
1123 <https://doi.org/10.1038/s41565-020-0648-y>

1124 Yan, H., Zhong, G., Xu, G., He, W., Jing, Z., Gao, Z., Huang, Y., Qi, Y., Peng, B., Wang, H., Fu,
1125 L., Song, M., Chen, P., Gao, W., Ren, B., Sun, Y., Cai, T., Feng, X., Sui, J., Li, W., 2012.
1126 Sodium taurocholate cotransporting polypeptide is a functional receptor for human
1127 hepatitis B and D virus. *eLife* 1, e00049. <https://doi.org/10.7554/eLife.00049>

1128 Yato, K., Onodera, T., Matsuda, M., Moriyama, S., Fujimoto, A., Watashi, K., Aizaki, H., Tanaka,
1129 T., Moriishi, K., Nishitsuji, H., Shimotohno, K., Tamura, K., Takahashi, Y., Wakita, T.,
1130 Muramatsu, M., Kato, T., Suzuki, R., 2020. Identification of Two Critical Neutralizing
1131 Epitopes in the Receptor Binding Domain of Hepatitis B Virus preS1. *J. Virol.*
1132 <https://doi.org/10.1128/JVI.01680-20>

1133 Ye, X., Zhou, M., He, Y., Wan, Y., Bai, W., Tao, S., Ren, Y., Zhang, X., Xu, J., Liu, J., Zhang, J.,
1134 Hu, K., Xie, Y., 2016. Efficient Inhibition of Hepatitis B Virus Infection by a preS1-binding
1135 Peptide. *Sci. Rep.* 6, 29391. <https://doi.org/10.1038/srep29391>

1136 Zhu, D.D., Zhang, X.P., Yu, H.L., Liu, R.X., Shen, C.B., Zhang, W.F., Cui, Y., Guo, X.D., 2019.
1137 Kinetic stability studies of HBV vaccine in a microneedle patch. *Int. J. Pharm.* 567,
1138 118489. <https://doi.org/10.1016/j.ijpharm.2019.118489>

1139